Research Paper

Upregulation of Haploinsufficient Gene Expression in the Brain by Targeting a Long Non-coding RNA Improves Seizure Phenotype in a Model of Dravet Syndrome

J. Hsiao [a], T.Y. Yuan [a], M.S. Tsai [b], C.Y. Lu [c], Y.C. Lin [a], M.L. Lee [d], S.W. Lin [b,e,f], F.C. Chang [c,g,h], H. Liu Pimentel [a], C. Olive [a], C. Coito [a], G. Shen [a], M. Young [a], T. Thorne [a], M. Lawrence [i], M. Magistri [j], M.A. Faghihi [j], O. Khorkova [a], C. Wahlestedt [j,*]

[a] OPKO Health Inc., 10320 USA Today Way, Miramar, FL 33025, USA
[b] Department of Clinical Laboratory Sciences and Medical Biotechnology, National Taiwan University Hospital, College of Medicine, National Taiwan University, No. 1, Sec. 1, Jen-Ai Rd., Taipei 100, Taiwan
[c] Department of Veterinary Medicine, School of Veterinary Medicine, National Taiwan University, No. 1, Sec. 4, Roosevelt Road, Taipei 106, Taiwan
[d] Dep. Clinical Laboratory Science and Medical Biotechnology, National Taiwan University Hospital, College of Medicine, National Taiwan University, Taipei, Taiwan
[e] Department of Laboratory Medicine, National Taiwan University Hospital, College of Medicine, National Taiwan University, No. 7, Chung-Shan S. Rd., Taipei 100, Taiwan
[f] Center for Genomic Medicine, National Taiwan University, No. 7, Chung-Shan S. Rd., Taipei 100, Taiwan
[g] Graduate Institute of Brain and Mind Sciences, College of Medicine, National Taiwan University, No. 1, Sec. 1, Jen-Ai Rd., Taipei 100, Taiwan
[h] Graduate Institute of Acupuncture Science, College of Chinese Medicine, China Medical University, Taichung, Taiwan
[i] RxGen, 100 Deepwood Drive, Hamden, CT 06517, USA
[j] Center for Therapeutic Innovation and the Department of Psychiatry and Behavioral Sciences, University of Miami Miller School of Medicine, 1501 NW 10th Avenue, Miami 33136, FL, USA

ARTICLE INFO

ABSTRACT

Dravet syndrome is a devastating genetic brain disorder caused by heterozygous loss-of-function mutation in the voltage-gated sodium channel gene SCN1A. There are currently no treatments, but the upregulation of SCN1A healthy allele represents an appealing therapeutic strategy. In this study we identified a novel, evolutionary conserved mechanism controlling the expression of SCN1A that is mediated by an antisense non-coding RNA (SCN1ANAT). Using oligonucleotide-based compounds (AntagoNATs) targeting SCN1ANAT we were able to induce specific upregulation of SCN1A both in vitro and in vivo, in the brain of Dravet knock-in mouse model and a non-human primate. AntagoNAT-mediated upregulation of Scn1a in postnatal Dravet mice led to significant improvements in seizure phenotype and excitability of hippocampal interneurons. These results further elucidate the pathophysiology of Dravet syndrome and outline a possible new approach for the treatment of this and other genetic disorders with similar etiology.

© 2016 The Authors. Published by Elsevier B.V. This is an open access article under the CC BY-NC-ND license (http://creativecommons.org/licenses/by-nc-nd/4.0/).

1. Introduction

Currently there is no treatment for many genetic disorders associated with loss-of-function mutations in one of the copies of a single gene (haploinsufficiency). Dravet syndrome (DS) is one of such disorders. DS is caused by heterozygous mutations in the SCN1A gene coding for the pore-forming alpha subunit of the voltage-gated sodium channel $Na_v1.1$. Clinically, DS is characterized by seizure onset in the first year of life, febrile seizures, prolonged seizures resistant to anticonvulsants, progressive psychomotor retardation and high incidence of sudden unexpected death (Dravet, 2011). Importantly, in most studied DS cases no mutant protein is produced and the characteristics of the Nav1.1-mediated sodium current are not significantly altered. However, the amplitude of the sodium

current and SCN1A mRNA and protein levels are diminished (Sugawara et al., 2003; Vanoye et al., 2006; Ohmori et al., 2006; Bechi et al., 2011). Although significant insights into DS disease mechanism have been achieved in recent years, it is still not clear if major manifestations of the disease are caused by disturbances in embryonic development or by persistent SCN1A deficiency in later life. It is also not known if increasing SCN1A expression after birth, when most genetic diseases are diagnosed, would alter the disease phenotype. Arguably the therapeutically required increase in SCN1A should not be very high, because just doubling the expression in haploinsufficient cells would restore the normal levels of the protein. In addition, excessive sodium currents, for example in cases of genomic duplications of sodium channel genes, also lead to seizures (Goeggel Simonetti et al., 2012; Yoshitomi et al., 2015).

To explore the effects of postnatal upregulation of SCN1A expression in Dravet syndrome, we took advantage of a novel long non-coding RNA(lncRNA)-based mechanism of gene regulation which, as we

* Corresponding author.
E-mail address: CWahlestedt@med.miami.edu (C. Wahlestedt).

show below, controls the expression of SCN1A mRNA. This mechanism is mediated by a lncRNA from the natural antisense transcript (NAT) class, which we named SCN1ANAT. Similar to other NATs (Katayama et al., 2005; Derrien et al., 2012), SCN1ANAT is a multi-exonic lncRNA transcribed from the opposite strand of the SCN1A gene (Fig. 1). SCN1ANAT shares small overlaps with the SCN1A coding sequences in both human and mouse genomes. NATs are known to function as fine modulators of on-going transcription, affecting a single gene or a small subset of related genes (Wahlestedt, 2013; Nakagawa and Kageyama, 2014; Zhao et al., 2010; Davidovich et al., 2013; Yu et al., 2015). The mechanisms of this gene-specific regulation likely involve tethering/ scaffolding of general-purpose epigenetic complexes at a particular gene locus (Magistri et al., 2012; Khalil et al., 2009; Peschansky and Wahlestedt, 2014). Methylation and other modifications of histones and DNA deposited by these complexes trigger chromatin compaction and transcriptional inhibition. Depleting NAT molecules or blocking their interaction with epigenetic complexes and DNA, or in essence inhibiting the inhibitor, leads to upregulation of their target protein coding genes (Katayama et al., 2005; Meng et al., 2015; Chung et al., 2011; Halley et al., 2014; Modarresi et al., 2012; Matsui et al., 2013; Yamanaka et al., 2015). Several epigenetic protein complexes have been shown to depend on NATs for their specificity (Nakagawa and Kageyama, 2014; Khalil et al., 2009; Kotake et al., 2011; Zhao et al., 2010). For example,

interfering with BDNF NAT function using synthetic oligonucleotide-based compounds (AntagoNATs) resulted in reduced levels of methylated lysine 27 in histone 3 in BDNF locus, reduced binding of a PRC2 component at the BDNF promoter, and increased expression of biologically active BDNF protein (Modarresi et al., 2012). Furthermore, blocking APOA1 NAT caused significant changes in histone H3 methylation levels and affected expression of several genes in the APOA1 cluster (Halley et al., 2014). In another example, a NAT from Lrp1 locus was shown to directly inhibit the activity of Hmgb2, a protein known to enhance the transcription of Lrp1. Oligonucleotides targeting Lrp1 NAT lifted its inhibitory interaction with Hmgb2 protein and increased Lrp1 expression (Yamanaka et al., 2015). Such DNA-level mechanisms enable NATs, frequently present in very low copy numbers, to efficiently control transcription at a given locus. As a consequence of their mechanism of action, the inhibitory activity of NATs is highly specific: it is limited to particular genes and engages only in cell populations that normally express their target coding genes (Magistri et al., 2012, Halley et al., 2014; Modarresi et al., 2012). Overall, NAT-mediated regulation is likely more suited to cases of haploinsufficiency than viral gene transfer, which often induces significant overexpression, is only partially responsive to endogenous controls, and has multiple technical and regulatory problems in the clinic. NAT-mediated regulation is present in many gene loci and is potentially applicable to the treatment of multiple genetic disorders

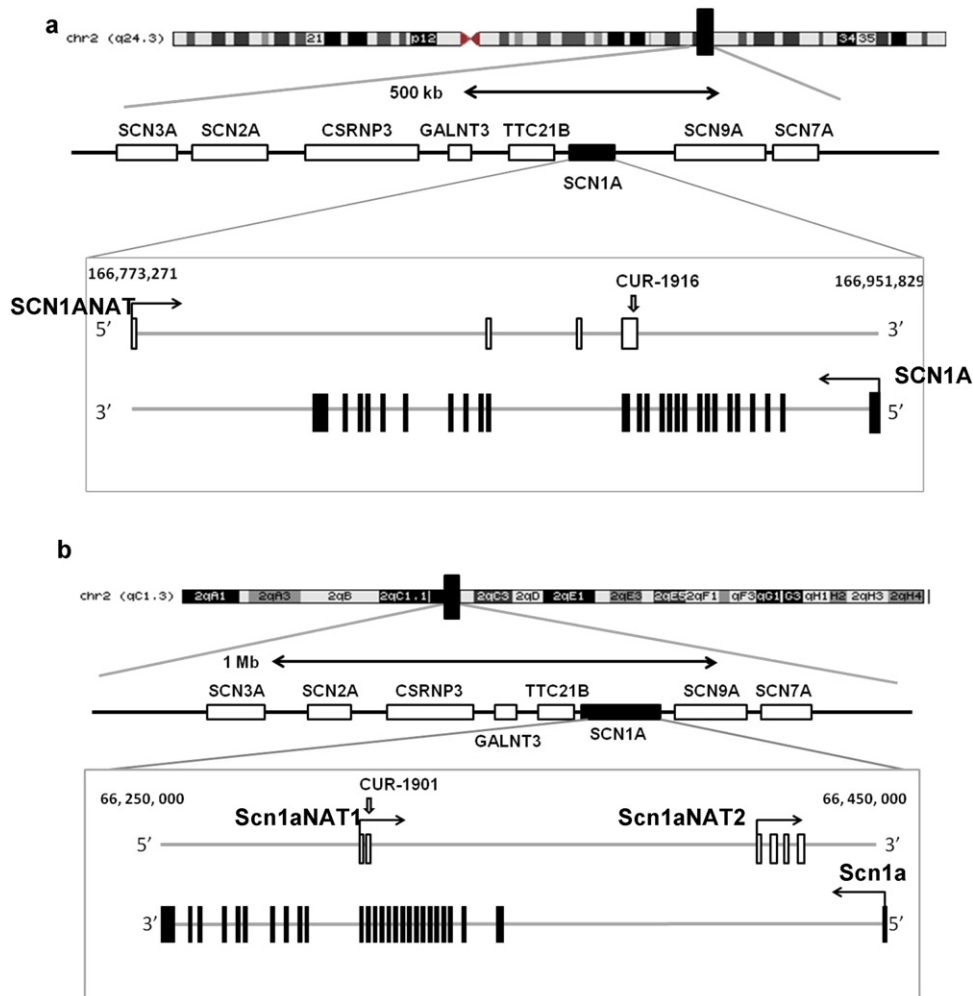**Fig. 1.** SCN1A and SCN1ANAT coding regions are localized on opposite chromosomal strands in human and mouse genomes. (a) Human chromosome 2. (b) Mouse chromosome 2. In the insets: empty boxes — SCN1ANAT exons; filled boxes — SCN1A exons; grey lines — complementary chromosomal strands; angled arrows — direction of transcription; CUR-1916, CUR-1901 — positions of sequences complementary to respective AntagoNATs.

(Wahlestedt, 2013). Given these attributes, NATs represent attractive targets for multiple diseases requiring protein upregulation, including DS.

2. Materials and Methods

2.1. Cell Lines

Human neuroblastoma cell line SK-N-AS (ATCC # CRL-2137™), African green monkey kidney epithelial cell line Vero 76 (ATCC # CRL-1587 ™), embryonic fibroblasts from the NIH/Swiss mouse 3T3 (ATCC # CRL-1658™) and brain neuroblastoma line from strain A albino mouse Neuro2A (ATCC # CCL-131™) were obtained from American Type Culture Collection (USA). SK-N-AS cells were cultured in DMEM with 10% FBS and 1% of penicillin/streptomycin. Vero76 cells were cultured in DMEM with 5% FBS and 1% of penicillin/streptomycin. 3T3 cells were cultured in Dulbecco's Modified Eagle's Medium with 10% FBS and 1% of penicillin/streptomycin. Neuro-2A cells were cultured in Eagle's Minimum Essential Medium with 10% FBS and 1% of penicillin/streptomycin. Experiments were performed within the first 15 passages after receipt form ATCC.

2.2. Introduction of Dravet Fibroblasts Into Culture

The skin biopsies for fibroblast lines D-01 to D-04 were collected at Surgery Center of Weston (Ft. Lauderdale, FL). All research subjects have signed informed consent forms. One skin biopsy per patient (~1 cm^3) was taken from the buttocks and placed in DMEM/F-12 (Ham) 1:1 media with 1% of penicillin/streptomycin. The skin was separated from subcutaneous fat, cut into pieces smaller than 1 mm^3, aliquoted into 6 tubes each containing 6 ml of DMEM/F-12 (Ham) 1:1 media with 1% of penicillin/streptomycin and 4 mg of collagenase and placed in a cell culture incubator. Twenty hours later the cells from each tube were centrifuged, the pellet resuspended in 5 ml of DMEM/F-12 (Ham) 1:1 media with 20% fetal bovine serum and 1% penicillin/streptomycin (growth media) and plated in a 6-well plate. Twenty four hours later the media was discarded and fresh growth media was added to each well. When the cells reached 80–90% confluency, the cells from each well were trypsinized and transferred to a T25 flask. When the cells reached confluence in the T25 flasks, all cells from one biopsy were pooled and seeded in 4xT75 flasks. The cells were maintained with weekly 1:2–1:3 splits. All experiments were done with cells from passages 4–20.

2.3. AntagoNAT Transfection

Cells were grown in appropriate growth media at 37 °C and 5% CO_2. One day before transfection the cells were replated at the density of 1.5×10^5/ml into 6 well plates and incubated at 37 °C and 5% CO_2. On the day of the transfection the media in the 6 well plates was changed to fresh growth media. All AntagoNAT sequences were tested against human genome and only ones with a single hit were chosen for extended investigation (sequences in table below). Lyophilized AntagoNATs synthesized by IDT were diluted to the concentration of 20 μM. Two μl of this solution were incubated with 400 μl of Opti-MEM media (Gibco, USA) and 4 μl of Lipofectamine 2000 (Invitrogen, USA) at room temperature for 20 min and applied to each well of the 6 well plates with cells. Similar mixture including 2 μl of water instead of the AntagoNAT solution was used for the mock-transfected controls. After 3–18 h of incubation at 7 °C and 5% CO_2 the media was changed to fresh growth media. Forty eight hours after addition of AntagoNATs the media was removed and RNA was extracted from the cells using SV Total RNA Isolation System from Promega or RNeasy Total RNA Isolation kit from Qiagen (cat# 74181) following the manufacturers' instructions.

1	T*C*G* G*T*G* T*C*C* A*C*T* C*T*G* G*C*A* G*T
2	T*G*C* A*C*T* G*T*G* G*G*A* G*C*C* T*G*T* C*T
3	G*T*A* G*C*A* C*T*G* T*G*G* A*C*A* T*C*G* G*C
4	G*T*A* G*A*A* G*A*A* C*A*G* C*C*C* G*T*A* G*T*G
5	G*T*G* G*T*C* T*C*T* G*C*A* T*T*C* T*G*T* C*A
6	G*T*G* G*T*A* T*A*G* G*A*A* C*T*G* G*C*A* G*C*A
7	G*T*C* C*A*A* T*C*A* T*A*C* A*G*C* A*G*A* A
8	G*T*G* A*C*T* G*T*A* C*C*A* A*T*T* G*C*T* G*T
9	A*C*T* T*C*T* T*C*C* A*C*T* C*C*T* T*C*C* T
10	G*A*T* G*T*C* C*C*T* T*C*C* T*G*C* G*T*T* G*T
11	T*G*T* G*G*A* T*G*C* T*G*G* G*T*G* T*C*T* C*T*C
12	T*C*C* C*A*G* T*G*A* C*T*C* C*C*G* A*T*G* C*T
13	A*G*T* C*T*C* A*G*T* T*G*T* C*A*G* T*A*C* C*T*C
14	G*T*T*A*T*T*G*A*A*T*G*C*C*T*G*T*G*T*G*T
15	T*C*G*G*A*T*C*A*T*C*A*G*G*G*T*T*G*T*A*G*T
CUR-1740	G*T*G*G*T*A*T*A*G*G*A*A*C*T*G*G*C*A*G*C*A
17	T*C*T*G*C*T*C*T*T*C*C*C*T*A*C*A*T*T*G*G
18	G*T*A*A*T*C*T*G*C*T*C*T*T*C*C*C*T*A*C
19	G*G*C*A*G*A*A*C*T*T*G*A*G*A*G*C*A*A*C*A*G
20	G*C*C*A*G*T*C*A*C*A*A*A*T*T*C*A*G*A*T*C*A
21	+C*+C*A*C*G*C*G*C*G*A*G*T*+A*+C*+A
22	+G*+T*A*T*A*G*G*A*A*C*T*G*+G*+C*+A
23	+G*+T*G*G*T*A*+T*A*G*G*A*A*+C*+T*+G
24	mG*mU*mG*G*mU*A*mU*A*G*G*A*A*mC*T*G*G*mC*A*mG*mC*mA
25	+A*+G*A*A*C*T*T*G*A*G*A*G*+C*+A*+A
26	mG*mG*mG*A*G*A*A*mC*T*mU*G*A*G*A*G*mC*A*A*mC*mA*mG
27	+G*+C*C*A*G*+T*C*A*+C*A*A*A*+T*+T*+C
28	+C*+A*C*A*A*A*T*T*C*A*G*A*+T*+C*+A
CUR-1770	mG*mC*mC*A*G*T*mC*A*C*A*A*A*mU*T*mC*A*G*A*mU*mC*mA
30	rArUrU rUrArA rArCrA rCrGrG rArArG rArCrU rUrUrA rGrUrA rGrUrG rCrUrA rCrUrA rArArG rUrCrU rUrCrC rGrUrG rUrUrU rArAA T
31	rUrCrA rCrArA rArUrU rCrArG rArUrC rArCrC rCrArU rCrUrU rCrUrA rGrArA rGrArU rGrGrG rUrGrA rUrCrU rGrArA rUrUrU rGrUG A
32	+G*+T*+T*GGTA+T*AGGAA+C*+T*+G
CUR-1837	mG*mU*mG*G mU*A mU*A G G A A mC*T G G mC*AmG*mC*mA

(continued)

34	+G*+C*CAGT*C*A+C*AAA+T*+T*+C
35	+C*+A*CAAATTCAGA+T*+C*+A
36	mG*mG*mU*A*mU*A*G*G*mA*A*C*mU*G*G*mC*A*G*mC*A*G*mU*G*mU*mU*mG
37	mU*mG*mG*T*A*mU*A*G*mG*A*A*mC*T*G*G*mC*A*G*C*mA*mG*mU
38	mG*G*T*A*mU*A*G*G*A*A*mC*T*G*G*mC*A*G*mC*A*G*T*G*T*T*mG
39	mA*mA*G*mC*G*G*mU*A*T*A*G*G*A*A*mC*T*G*G*mC*A*G*mC*A*mG
40	G*T*G*G*C*A*T*A*G*G*G*A*C*G*G*G*C*A*G*C*A
CUR-1916	mG*mA*mG*C*C*A*G*mU*C*A*mC*A*A*A*mU*T*C*A*G*mA*T*C*A*mC*mC*mC
42	mA*A*mU*G*G*G*A*G*A*A*mC*mU*mU*G*A*G*A*G*mC*mA*mA
43	G*T*G*GAC*AGGAT*GCAC*AAAGG*A
44	mG*TGACmU*GTGCCmC*ATTGCTmG
45	mG*ACAAmC*CTTGmC*AGCCAmC*TGAmU*GATGmA
46	T*G*G*T*A*T*A*G*G*A*A*C*T*G*G*C*A*G*C*A
47	mU*mG*G*mU*A*mU*A*G*A*A*mC*T*G*G*mC*A*mG*mC*mA
48	mC*mC*A*G*T*mC*A*C*A*A*A*mU*T*mC*A*G*A*mU*mC*mA
49	mU*mG*G mU*A mU*A G G A A mC*T G G mC*AmG*mC*mA
50	mA*mG*C*C*A*G*mU*C*A*mC*A*A*A*mU*T*C*A*G*mA*T*C*A*mC*mC*mC
51	mG*mC*C*A*G*mU*C*A*mC*A*A*A*mU*T*C*mA*mG
52	mG*mC*C*A*G*mU*C*A*mC*A*A*A*mU*mU*mC
53	+G*+C*C*A*G*mU*C*A*mC*A*A*mA*mU*+T*+C
54	+G*C*C*A*G*+T*C*A*+C*A*A*T *+T*+C
55	+G*+C*mC*A*G*mU*C*A*mC*A*mA*+A*+T
CUR-1945	+G*+C*C*A*G*T*C*A*C*A*+A*+A*+T
57	+G*C*C*A*G*T*C*A*+C*+A*+A
58	+G*+C*C*A*G*T*C*A*C*+A*+A*+A
59	+A*+T*T*G*A*G*C*C*A*+G*+T*+C
60	TCGACTTTGAAAA
61	CCTCTCCACGCGCAGTACATT
62	G*T*A* G*C*A* C*T*G* T*G*G* A*C*A* T*C*G* G*C
63	G*T*A* G*A*A* G*A*A* C*A*G* C*C*C* G*T*A* G*T*G
64	G*T*C* C*A*A* T*C*A* T*A*C* A*G*C* A*G*A* A
65	G*T*G* A*C*T* G*T*A* C*C*A* A*T*T* G*C*T* G*T
66	A*C*T* T*C*T* T*C*C* A*C*T* C*C*T* T*C*C* T
67	G*A*T* G*T*C* C*C*T* T*C*C* T*G*C* G*T*T* G*T
68	T*G*T* G*G*A* T*G*C* T*G*G* G*T*G* T*C*T* C*T*C
69	T*C*C* C*A*G* T*G*A* C*T*C* C*C*G* A*T*G* C*T
70	A*G*T* C*T*C* A*G*T* T*G*T* C*A*G* T*A*C* C*T*C
71	T*C*G*G*A*T*C*A*T*C*A*G*G*G*T*T*G*T*A*G*T
72	G*T*G*G*T*A*T*A*G*G*A*A*C*T*G*G*C*A*G*C*A
73	+G*+T*A*T*A*G*G*A*A*C*T*G*+G*+C*+A
74	+G*+T*G*G*T*A*+T*A*G*G*A*A*+C*+T*+G
75	mG*mU*mG*G*mU*A*mU*A*G*G*A*A*mC*T*G*G*mC*A*mG*mC*mA
76	rArUrU rUrArA rArCrA rCrGrG rArArG rArCrU rUrUrA rGrUrA rGrUrG
	rCrUrA rCrUrA rArArG rUrCrU rUrCrC rGrUrG rUrUrU rArAA T
77	+G*+T*GGTA+T*AGGAA+C*+T*+G
78	mG*mU*mG*G mU*A mU*A G G A A mC*T G G mC*AmG*mC*mA
79	mG*mG*mU*A*mU*A*G*G*mA*A*C*mU*G*G*mC*A*G*mC*A*G*mU*G*mU*mU*mG
80	mU*mG*mG*T*A*mU*A*G*mG*A*A*mC*T*G*G*mC*A*G*C*mA*mG*mU
81	mG*G*T*A*mU*A*G*G*A*A*mC*T*G*G*mC*A*G*mC*A*G*T*G*T*T*mG
82	mA*mA*G*mC*G*G*mU*A*T*A*G*G*A*A*mC*T*G*G*mC*A*G*mC*A*mG
83	G*T*G*G*C*A*T*A*G*G*G*A*C*G*G*G*C*A*G*C*A
CUR-1901	mG*mU*mG*G*mC*A*mU*A*G*mG*G*A*mC*G*G*G*mC*A*mG*mC*mA
85	mA*mC*mA*mA*mG*mU*G*C*A*T*A*G*G*G*A*C*G*G*G*mG*mC*mA*mG*mC*mA
86	mA*mC*A*A*G*mU*G*G*mC*A*T*A*mG*G*G*A*mC*G*G*G*mC*A*G*mC*mA
87	mA*A*G*mU*G*G*mC*A*mU*A*G*mG*G*A*mC*G*G*G*mC*A*G*mC*A*G*mU
88	mA*mA*mG*mU*mG*G*C*A*T*A*G*G*A*C*G*G*G*C*A*mG*mC*mA*mG*mU
89	G*T*G*ACTGTGCCCATTG*C*T*G
90	G*C*C*ACTT*GATGAT*CTA*A*A*C
CUR-1924	G*T*G*GAC*AGGAT*GCAC*AAAGG*A
92	mG*TGACmU*GTGCCmC*ATTGCTmG
93	mG*TGACTGTGCCCATTGCTmG
94	mC*CTCmU*TTCmU*GGCmC*TTGmC*TTmC
95	mG*ACAAmC*CTTGmC*AGCCAmC*TGAmU*GATGmA
96	T*G*G*T*A*T*A*G*G*A*A*C*T*G*G*C*A*G*C*A
97	mU*mG*G*mU*A*mU*A*G*G*A*A*mC*T*G*G*mC*A*mG*mC*mA
CUR-1462	mC*mC*mU*mA*mU*mC*T*T*T*C*C*C*C*C*C*C*T*mA*mC*mC*mU*mU*mU

* — phosphorothioate bond, m — 2′OMethyl modification, + — LNA modification, r — ribonucleotide.

2.4. Quantitative Real Time PCR

2.4.1. RNA Extraction

Cultured cells were lysed inside the plates using SV total RNA kit (Promega, WI USA). Mouse and monkey tissues were weighed and up to 30 mg per sample were placed in 2 ml lysis matrix D tubes (MP Bio-medicals, CA USA). The tissues were homogenized in RLT buffer (Qiagen, USA) using an MP FastPrep24 homogenizer (MP Biomedicals, CA USA). Cell or tissue lysates were centrifuged to remove debris and loaded onto nucleic acid-binding columns from respective RNA extraction kits. After several washes the bound RNA was subjected to DNAse treatment directly on the column and then the total RNA was eluted in DNAse/RNAse free water. RNA concentration was determined using Multiskan spectrophotometer (Thermo Scientific, USA).

2.4.2. Reverse Transcription

100–500 ng of total RNA was used per reverse transcription reaction. The complementary DNAs were synthesized using High Capacity cDNA Reverse Transcription Kit (Applied Biosystems, USA) or SuperScript Vilo cDNA Synthesis Kit (Life Technologies) according to manufacturers' protocols.

2.4.3. Quantitative Real Time PCR

cDNA was PCR amplified using TaqMan Fast Advance Master Mix and TaqMan® Gene Expression Assays labeled with FAM (Hs00374696_m1 specific for human or Mm00450580_m1 assay specific for mouse Scn1a RNA; assays for human SCN2A — Hs00221379_m1, SCN3A — Hs00366902_m1, SCN5A — Hs00165693_m1, SCN7A — Hs00161546_m1, SCN8A — Hs00274075_m1, SCN9A — Hs00161567_m1, mouse SCN9A — Mm00405762_S1, custom assay for human SCN1ANAT — context sequence GGAAACACCACAGCATAGTGATTAG, assay for mouse Scn1aNAT Mm01329045_mH) in a StepOne Plus analyzer (all from Applied Biosystems, USA). For mouse Scn1aNAT assay RT was conducted with sequence-specific primers (sequences shown below, synthesized by IDT Inc.). The levels of 18S rRNA were estimated as an internal control, using a TaqMan® Gene Expression Control labeled with VIC (Mm03928990_g1 for mouse, Hs99999901_s1 for human and monkey, all from Applied Biosystems, USA). The analysis of the data was done using Excel software.

2.4.4. Quantitative Real Time PCR for Mutant and WT Alleles

Custom mutant and wild type allele assays for D-00 and D-02 mutations were manufactured by Thermo Fisher Scientific. Copy numbers were estimated using calibration standards synthesized by IDT Inc. (sequences shown below).

2.5. Immunohistochemistry

Cells were grown in 24 well plates and treated with AntagoNATs as described above. Forty-eight hours after dosing, cells were fixed with 100% methanol at −20 °C for 15 min followed by several PBS washes. The cells were then treated at room temperature with 3% hydrogen peroxide, blocked in 5% normal goat serum and avidin/biotin, then incubated overnight at 4 °C with rabbit polyclonal anti-SCN1A antibody (Alomone Labs, Israel, cat# ASC-001, validation information at http://www.alomone.com/p/anti-nav1.1/asc-001/44, accessed 01.16.15) diluted 1:250, or rabbit polyclonal IgG (Abcam) diluted to 1:250 or 1:500, or rabbit polyclonal anti-actin antibody (Abcam, UK) diluted 1:500. Then the cells were incubated with goat anti-rabbit antibody (Vectastain Elite ABC kit, Rabbit IgG, Vector Labs, USA) for 1 h followed by 30 min with reagents A and B from Vectastain Elite ABC kit. The cells were then incubated with ImmPACT DAB until the development of the staining. The staining of the cells was analyzed directly inside the wells using an inverted Nikon Eclipse TS100 microscope equipped with a Nikon DS-Ri1 camera coupled to Nikon Digital Sight equipment and a Dell Latitude D630 laptop. For each condition there were at least 3 biological replicates. The photographs of the stained cells were converted into black-and-white negative images using the NIS-Elements D 3.0 software. For each well, 4 sections of the same size were quantified using the NIS-Elements D 3.0 software tools. Statistical analysis was done using Excel software.

2.6. Sequencing of SCN1A NAT

Candidate SCN1ANAT was identified based on transcriptome database data related to SCN1A locus. Candidate transcripts were encoded by the chromosome strand opposite to SCN1A and overlapped SCN1A gene. Empirical confirmation of these findings was performed to validate the regulatory effects of these transcripts on SCN1A expression. The bacterial clone from which the database sequence was obtained was purchased from Open Biosystems (http://www.openbiosystems.com/; clone ID 4829512). Ten colonies were picked and grown in 5 ml of LB broth containing ampicillin at 100 μg/ml. The plasmid was extracted using PureYield™ Plasmid Miniprep System (Promega, USA) following the manufacturer's protocol and bidirectionally sequenced at Davis Sequencing (USA) using T3 and T7 primers.

2.7. RACE

Total RNA was extracted from HepG2 cells or primary Dravet fibroblasts using the QIAGEN RNeasy Midi Kit (QIAGEN, USA) as described by the manufacturer. PolyA RNA was isolated with the Poly(A)Purist™ MAG Kit and eluted twice with 200 μl of THE RNA Storage Solution (Ambion, USA).

2.7.1. 3′ End RACE

One μg of total RNA or total RNA polyadenylated using Ambion® Poly(A) Polymerase (Ambion, USA) or 50 ng of polyA RNA was reverse transcribed using FirstChoice® RLM RACE Kit (Ambion, USA). One μl of the RT reaction was PCR amplified using 5′ GATTCTCCTACAGCAATTGGTA 3′ as the specific oligonucleotide. Using 1 μl of the first PCR reaction, a second PCR was done using 5′ GACATGTAATCACTTTCATCAA 3′ as specific oligonucleotide following the FirstChoice® RLM RACE Kit protocol.

2.7.2. 5′ End RACE

Ten microgram of total RNA or total RNA polyadenylated using Poly(A) Polymerase (Ambion, USA) or 250 ng of polyA RNA were treated with calf intestine alkaline phosphatase from the FirstChoice® RLM RACE Kit (Ambion, USA), followed by phenol/chloroform RNA

Name	Sequence
RTprimerNAT-1	CCTTACTGTCTTCATGATGGTCA
RTprimerNAT-2	GCATGCAGCTGTTTGGAA
RTprimerNAT-3	GACTTCTTC CACTCGTTCCT
RTprimerNAT-4	GTTACAAAGATTGTGTCTGCAA
RTprimerMRNA-1	CCCGTCCCTATGCCACTTGT
RTprimerMRNA-2	GTCAGACTCTCCCACAGCA
RTprimerMRNA-3	GTCTACTGTGCTTCCCTCTGA
RTprimerMRNA-4	GTACTTCTCCACACTGCTGCC
Calibration Standard D00WT	TGATCTAAACAACAAGAAAGACAGTTGTATGTCCAATCATACAGCAGAAATTGGGAAAGATCTTGACTATCTTAAAGATGTAAATGGAACTACAAGTGGTATAGGA ACTGGCAGCAGTGTTGAAAAATACATTATTGATGAAAGTGATTACATGTCATTCATAAACAACCCCAGTCTTACTGTGACTGTACCAATTG
Calibration Standard D00mu	TGATCTAAACAACAAGAAAGACAGTTGTATGTCCAATCATACAGCAGAAATTGGGAAAGATCTTGACTATCTTAAAGATGTAAATGGAACTACAAGTGGTATAGGA ACTGGCAGCAGTGTTGAAAAATACATTATTGATTAAAGTGATTACATGTCATTCATAAACAACCCCAGTCTTACTGTGACTGTACCAATTG
Calibration Standard D02WT	GGGAAAATCTTTATCAACTGACATTACGTGCTGCTGGGAAAACGTACATGATATTTTTTGTATTGGTCATTTTCTTGGGCTCATTCTACCTAATAAATTTGATCCTGGCT GTGGTGGCCATGGCCTACGAGGAACAGAATCAGGCCACCTTGGAAGAAGCAGAACAGAAAGAGGCCGAA
Calibration Standard D02mu	GGGAAAATCTTTATCAACTGACATTACGTGCTGCTGGGAAAACGTACATGATATTTTTTGTATTGGTCATTTTCTTGGGCTCATTCTACCTAATAAATTTGATCCTGGCTG TGGTGGCCATGGCCTACGAGGAACAGAATCAGGCCACCTTGGAAGAAGCAGAACAGAAAGAGGCCGAA

extraction, isopropanol precipitation and treatment with tobacco acid pyrophosphatase to remove any CAP structures. At this time, an oligonucleotide adapter was covalently linked to the 5′ end of the RNA. Using 2 μl of the linked RNA, a reverse transcription using FirstChoice® RLM RACE Kit (Ambion, USA) was performed at 42 °C for 1 h. One μl of the RT reaction was PCR amplified using 5′ GTGGAACCTGAAGAAACTCTTG 3′ as specific oligonucleotide. Using 1 μl of the first PCR reaction, a second PCR was done using 5′ GTCCACTCTGGCAGTGCTTGAG 3′ as specific oligonucleotide following the FirstChoice® RLM RACE Kit protocol.

2.7.3. cDNA Cloning

One microliter of second PCR reaction from the 3′ end or 5′ end RACE was ligated into a T easy vector (Promega, USA). One microliter of the ligation reaction was added to OneShot Top10 competent cells (Invitrogen, USA) using heat shock procedure. One hundred clones were picked and grown in 5 ml of LB broth containing ampicillin at 100 μg/ml. The plasmid was extracted using PureYield™ Plasmid Miniprep System (Promega, USA) following the manufacturer protocol. The inserts were bidirectionally sequenced by Davis Sequencing (USA) using SP6 and T7 primers.

2.8. RNAseq Experiments

SK-N-AS cells were treated with 20 nM of active AntagoNAT CUR-1916 or control oligonucleotide CUR-1462 ($n = 3$/group) and RNA was extracted as described above. Template DNA molecules suitable for cluster generation were prepared from 500 ng of total RNA per sample using the TruSeq RNA Sample Preparation Kit v2 (part # RS-122-2001, Illumina Inc., San Diego, CA) according to the manufacturer's instructions. The size distribution of the libraries was estimated by bioanalysis using the Caliper LabChip GX system (PerkinElmer; Waltham, MA). The mean size for the libraries was approximately 348 ± 3 nucleotides. Libraries were quantified using the KAPA Library Quantification Kit (Part # KK4824, Kapa Biosystems; Boston, MA). The libraries were pooled at equimolar concentrations and diluted prior to loading onto the flow cell of the cBot cluster station (Illumina Inc.; San Diego, CA). The libraries were extended and bridge amplified to create single sequence clusters using the HiSeq PE Cluster Kit v4 cBot (Part # PE-401-4001, Illumina Inc., San Diego, CA). The flow cell carrying amplified clusters was loaded on the HiSeq 2500 sequencing system (Illumina Inc., San Diego, CA) and sequenced using the 50-nt paired-end plus index read sequencing protocol with reagents from the HiSeq SBS Kit v4 (Part # FC-401-4002, Illumina Inc.; San Diego, CA), sequencing primers from the HiSeq PE Cluster Kit v4, and an index read primer from the TruSeq Dual Indexing Sequencing Primer Kit (PE-121-1003). Real time image analysis and base calling were performed using the HiSeq Control Software version 2.2.58. CASAVA software version 1.83 was used to produce de-multiplexed FASTQ sequence files from raw .bcl files. Sequences were aligned to the human genome version hg19 (UC Santa Cruz) using TopHat v1.4.1. EasyRNASeq v1.6.0 running on the R version 3.0 platform was used for determination of raw reads and reads per kilobase per million reads (RPKM) for each gene and exon. Using a custom R script, further annotation information was added from Ensembl human version 72 table downloaded from Ensembl Biomart. Fold changes were calculated and statistical analysis was performed using R version 3.0 statistical software. False discovery rates (FDR) were calculated using the method of Benjamini and Hochberg. If the mean of both groups considered in a fold-change comparison were below the Reliable Detection Threshold (50 reads/gene), "NA" was reported. Differentially expressed genes were defined as genes with a more than 2-fold difference in expression with $p < 0.05$ and FDR < 0.05. Functional annotation of genes was performed using PubMed (http://www.ncbi.nlm.nih.gov/pubmed/, accessed April 15, 2015), Reactome (http://www.reactome.org/, accessed April 15, 2015), StarNet (http://vanburenlab.medicine.tamhsc.edu/starnet2.

shtml, accessed April 15, 2015) and neuronal/glial expression databases (Cahoy et al., 2008).

2.9. Generation of Mouse Model of Dravet Syndrome

The knock-in (KI) mouse strain Scn1aE1099X was generated in the laboratory of Dr. S.W. Lin (National Taiwan University) (Tsai et al., 2015). Briefly, a targeting vector was constructed using recombineering-based method (Liu et al., 2003). Initially, a 15 kb mouse genomic DNA encompassing exons 10–17 of the Scn1a gene was isolated from a 129/Sv DNA BAC clone (bMQ419a06, purchased from Source BioScience, Nottingham, UK) and subcloned into the NotI and SpeI sites of pL253. A 600-bp fragment containing exon 17 and its upstream and downstream sequence was subcloned into pL452 harboring a neomycin-resistance cassette surrounded by 2 loxP sites (Cre-recombinase recognition sequences for removal of the neo cassette). The nucleotide sequence, GAG, encoding glutamic acid at position 1099 in exon 17 was mutated to TAG (stop codon) by 4-primer PCR method. The resultant plasmid, pL452-E1099X, was used to insert the E1099X and the neo-2-loxP cassette into pL253. The resultant targeting vector, pL253-E1099X, allowed KI of the E1099X mutation and the neo-2-loxP cassette into the chromosome of the mouse embryonic stem cells. The pL253-E1099X targeting vector was linearized with NotI and electroporated into the R1 hybrid embryonic stem (ES) cells. The ES cell clones that survived G418 (240 mg/ml) and ganciclovir (2 μM) selections were further analyzed by Southern blotting for correct homologous recombination. Wild type (WT) and KI ES cell genomic DNA digested by BamHI restriction enzyme generate a 16.5-kb and a 15-kb fragment, respectively, when detected by a 3′ probe, and a 18.9-kb and a 12-kb fragment, respectively, when digested by AvaI and detected by a 5′ probe. To excise the neo cassette from the correctly targeted ES cell clones, the ES cell clones were electroporated with a Cre-expressing plasmid (pCX-PTD-Cre, constructed in house) that mediates excision of the loxP-floxed neo sequences. After transfection, surviving individual ES cell clones were isolated and their DNA screened by PCR using oligonucleotide primers Scn1a-20,571 U (5′-AGGGAGATGAATGCCAAAGC-3′) and Scn1a-20,930-2D (5′-GACAATTGGTAGGGAGCACT-3′) in a PCR reaction with the following conditions: 95 °C for 2 min, followed by 40 cycles of 95 °C for 30 s, 55 °C for 1 min and 72 °C for 1 min, and a final extension at 72 °C for 7 min. WT and the KI allele yielded a respective PCR products of 359 bp and 459 bp. The resultant KI ES cell clones were injected into C57BL/6JNarl blastocysts to establish chimeric mice for germ-line transmission of the Scn1a$^{E1099X/+}$ allele through breeding processes. Confirmation of germline transmission was performed by genotyping, sequencing, and Southern blotting of the genomic DNA of the first offspring of chimeric mice. Genotypes of subsequent generations were analyzed by PCR as described above. Mating of chimeras was conducted as follows. Generation I: offspring of chimeric mice [derived from RI (129 × 1 × 129S1) ES cells] mated with 129 female mice (129S2/SvPasCrl; Charles River). Generation II (N1F1): male offspring of generation I mated with C57BL/6JNarl (purchased from National Animal research Laboratory, Taiwan) female mice. Generation III (N2F1): male offspring of generation II mated with C57BL/6JNarl female mice. Animals were genotyped for the presence of the KI allele (Scn1a^{E1099X}) and uniquely identified by toe clipping displaying the animal number.

2.10. AntagoNAT Treatment and EEG Recording in Dravet Mice

Seven week old naïve Dravet mice were housed individually for duration of experiment. Food (5001 rodent diet, LabDiet) and water were offered ad libitum. Light/dark (12 h/12 h) cycle was maintained. Animals were assigned to different groups using the stratified randomization procedure based on gender, animal weight and age. All animal procedures were approved and controlled by the Taiwan National University ethics committee and carried out according to the institutional animal care and use guidelines. All experiments were planned and

carried out according to the NINDS guidelines for transparent data reporting (Landis et al., 2012).

2.10.1. EEG Electrode Implantation

Mice were anesthetized by intraperitoneal injection of Zoletil (4.13 mg/kg) and surgically implanted with two electroencephalogram (EEG) wire electrodes. Insulated leads from EEG electrodes were routed to a pedestal. The pedestal was then cemented to the skull with dental acrylic (Tempron, GC Co., Tokyo, Japan). The incision was treated topically with polysporin (polymixin B sulfate/bacitracin zinc) and the animals were allowed to recover for 6 days prior to the initiation of experiments. Ibuprofen (15 mg/100 ml) was added into the drinking water for two days after surgery. Four days after surgery, a tether was connected to the EEG electrodes.

2.10.2. EEG and Video Monitoring

EEG and video monitoring in these studies was conducted continuously 24 h a day every day for the whole period of AntagoNAT treatment (28–30 days) until animal sacrifice. EEG recordings were analyzed using Axoscope software by visually identifying the times of increased activity followed by a depression, and recording time of onset, duration and amplitude of each seizure episode. All instances of seizures identified by analysis of EEG traces were verified using video recordings. Seizure severity was graded based on EEG and video data according to the following scale: stage 3 — tremor in the front feet and back, rigidity in the tail, seizure amplitude on EEG 2 mV–3.5 mV; stage 4 — tremor in front and back legs and back, rigidity in the tail, mice are unable to maintain their standing posture and fall down, seizure amplitude 3.6 mV–4.5 mV; stage 5 — generalized tremors cause sudden jumps, seizure amplitude on EEG over 4.6 mV. EEG analysis was conducted by 2 independent observers blinded to the treatment.

2.10.3. Intrathecal Administration of AntagoNATs

AntagoNATs used in mouse studies were CUR-1901 and CUR-1924 (synthesized by IDT Inc.). CUR-1901 was administered once weekly for 4 weeks. Three microliters of AntagoNAT solution at desired concentration followed by 2 μl of saline vehicle were injected intrathecally using the method of Hylden and Wilcox (1980). Briefly, after mice were lightly anesthetized with ketamine (100 mg/kg) the spinal space was identified by inserting a 30-gauge needle at a 20″ angle cephalad between adjacent lumbar spinal processes (L5–6). Resistance encountered at a depth of approximately 5 mm indicated proper position of the needle tip within the spinal canal. AntagoNATs were injected slowly using a 100-PL syringe (Hamilton Co., Reno, NV). The L5–6 interspace approximates the termination of the spinal cord and the origins of the cauda equina. Injection at this site maximizes intervertebral accessibility and minimizes the likelihood of spinal cord damage. The animals remained under the influence of anesthetic for 2–7 h under continuing EEG and video recording. Correct targeting of the injection was confirmed using a dye solution.

2.11. Heat Induction of Seizures

Mice were placed in the transparent acrylic cylinder approximately 30 cm tall, 9 cm in diameter and 0.3 cm thick. An infrared heating lamp suspended approximately 10 cm over the top of the cylinder was used to pre-heat the cylinder for 15 min before experiment start, ensuring even temperature within the cylinder and in the surrounding area. The temperature was increased without thermal feedback, in 3 standard, pre-set steps 10/5/5 min long. Core body temperature was continuously recorded using a rectal probe (TD-300 NATSUME, Japan). Behavioral seizure start was defined as clonic forelimb cramps, stiffening of the body and shaking of the tail. At seizure start the lamp was turned off. Mice were then returned to home cage and closely monitored for several hours. Core body temperature at seizure start was

recorded as the threshold temperature. Mice were videotaped during heat induction.

2.12. Electrophysiological Experiments

2.12.1. Brain Slice Preparation

Acute hippocampal slices were prepared from mice of 5–6 weeks old. Briefly, mice were decapitated, and the brains were quickly removed and immersed in ice-cold oxygenated slicing solution containing (in mM): 250 sucrose, 2.5 KCl, 0.5 $CaCl_2$, 5 $MgCl_2$, 1.26 $NaHPO_4$, 26 $NaHCO_3$, and 15 glucose aerated to a pH of approximately 7.4 with 95% O_2–5% CO_2. Coronal brain slices (300 μm) were cut in cutting solution on a microslicer (DTK-1000, Dosaka, Kyoto, Japan) and transferred to a holding chamber containing artificial cerebrospinal fluid (ACSF) consisting of (in mM): 125 NaCl, 2.5 KCl, 2 $CaCl_2$, 1 $MgCl_2$, 1.26 $NaHPO_4$, 26 $NaHCO_3$, and 15 glucose aerated with 95% O_2 and 5% CO_2. The slices were then maintained at room temperature (23 ± 2 °C) for at least 1 h before recording.

2.12.2. Electrophysiological Eecordings

During recording, slices were placed in a recording chamber and continuously perfused with ACSF. Recordings were made at room temperature. The resistance of the patch electrode was 3–8 MΩ. Whole-cell patch-clamp recordings were acquired with an Axopatch 200B amplifier (Molecular Device, Foster City, CA). Nav1.1 is mainly expressed in parvalbumin (PV)-positive GABAergic interneurons of the brain (Ogiwara et al., 2007). PV-positive interneurons were recognized by their large soma (>30 μm) and location at the border of granule layer in the dentate gyrus and the typical fast-spiking firing patterns. The firing activity of PV-positive interneurons was recorded under current clamp using K-gluconate-based internal solution containing (in mM): 140 K-gluconate, 9 NaCl, 1 $MgCl_2$, 1 EDTA, 10 HEPES, 2 Mg-ATP, 0.3 Na-GTP and 10 biocytin, pH adjusted to 7.3 with KOH. After recording, slices containing biocytin-filled cells were fixed with 4% paraformaldehyde overnight at 4 °C and then reacted with Texas Red-avidin (1:200; VectorLab, Burlingame, CA) and rabbit anti-PV primary antibody (1:500, Millipore). The secondary antibody used was Cy5-conjugated anti-rabbit IgG (1:200, Jackson ImmunoResearch Laboratories). PV-positive recorded neurons displaying typical fast-spiking activity were collected for further analysis. The input-output function was determined by the action potential (AP) number in response to a series of depolarizing current pulses of 1 s. Data were acquired using Clampex 10.2 software (Molecular Devices), filtered at 5 kHz, digitized at 10 kHz, and recorded directly on the computer hard disk using AxoScope 10.2 software (Molecular Devices). Firing activity was analyzed using Clampfit 10.2 (Molecular Devices). Input resistance was calculated from the voltage difference between steady state and a 1-s long hyperpolarizing current injection of −50 pA. AP properties were measured from the first AP in the depolarizing protocol. The AP threshold was determined as the first point in the voltage trajectory with a slope change exceeding 20 V/s. The AP amplitude was measured from the threshold to the peak of the spike. The AP properties were measured from the first AP in the depolarizing protocol. The slopes were calculated during the 10–90% rise phase and the 90–10% decay phase of the AP. The AP half-width was measured at half-maximal amplitude. Afterhyperpolarization (AHP) was measured as the voltage difference between the threshold and the most negative voltage point in AP.

2.13. AntagoNAT Treatment in African Green Monkeys

The studies in African green monkeys (*Cercopithecus aethiops sabaeus*) were conducted by RxGen at the St. Kitts Biomedical Research Foundation, St. Kitts, West Indies. Animals were housed in a primate enclosure. Humidity and temperature of the housing enclosure was monitored for the duration of the study. All animal procedures were approved and controlled by the St. Kitts Biomedical Research
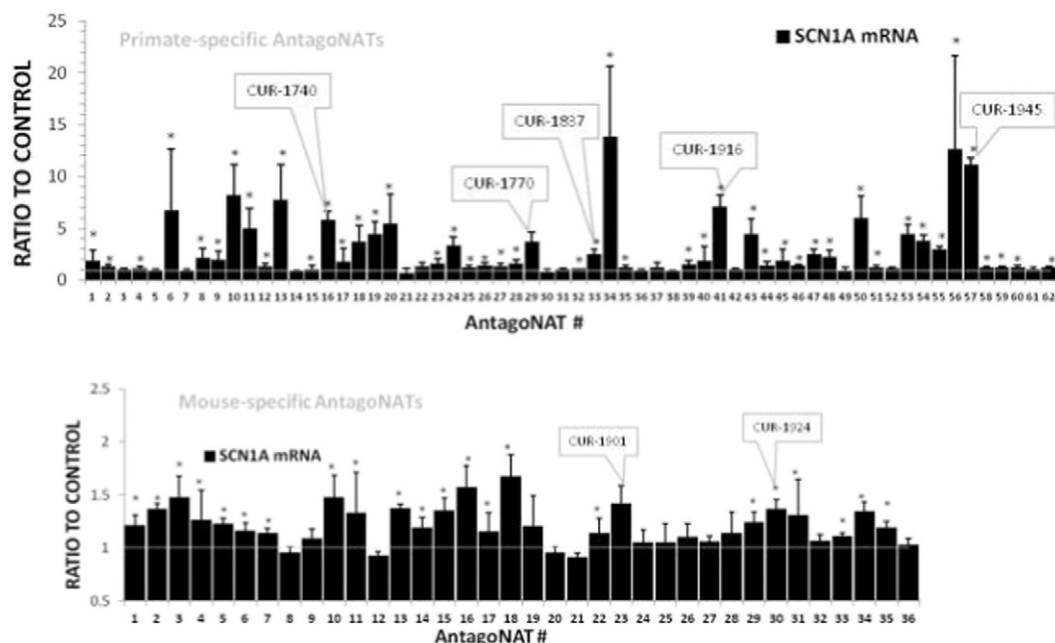
Foundation ethics committee and carried out according to the institutional animal care and use guidelines. All experiments were planned and carried out according to the NINDS guidelines for transparent data reporting (Landis et al., 2012). AntagoNATs CUR-1916, CUR-1740, CUR-1945, CUR-1837 and a control oligonucleotide CUR-1462 were used in these studies. AntagoNATs were synthesized by Ribotask ApS (Denmark) and BioSpring Gesellschaft für Biotechnolgoie mbH (Germany). Adult naïve male animals were allocated to groups by means of a stratified randomization procedure based on body weight. A single percutaneous CSF tap/infusion was conducted under ketamine/xylazine sedation [5.0 mg/kg ketamine (Fort Dodge)/1.0 mg/kg xylazine (Lloyd Lab) administered intramuscularly in a sterilely mixed cocktail]. Prior to CSF infusion monkeys were placed in a prone position with one study participant stabilizing the head in flexion. The test or

Table 1

Alignment of human (H), monkey (R) and mouse (M) Scn1aNATs. Nucleotides 721 to 1123 of human SCN1ANAT (shown in italics) were revealed by additional sequencing of clone 4,829,512 and RACE experiments. Context sequence for human/monkey SCN1ANAT gene expression assay is highlighted in bold, sequences complementary to AntagoNATs are underlined. Nucleotides 8–170 are derived from an LTR12E repeat (family ERV1).

```
H:1    agcggggggttcccgcccgcgcctctccctccacacctccccgcaagcagagggagccggctccggccttgg

R:     ----------------------------------------------------------------------

M:     ----------------------------------------------------------------------


H:73   ccagcccagagacaggctcccacagtgcagcggcgggctgaagggctcctcaagcactgccagagtggaca

R:     ----------------------------------------------------------------------

M:     ----------------------------------------------------------------------


H: 144 ccgaggccgaggagacgccaagagcga 170

R:     --------------------------

M:     --------------------------


H: 171 tgaaacaagcttctggttcaagagtttcttcaggttccactacgggctgttcttctacag 230
       ||||||| ||||| ||||||||| |||||||||||||||||||||||||||||||| |||
R: 1   tgaaacaggcttccggttcaagggtttcttcaggttccactacgggctgttcttctgcag 60
       |||| || |||||| || ||||| |||||||| ||||| | || ||||||| ||| |||
M: 1   tgaagcaagcttcgggctcaagggtttcttctggttcaatgacaggctgttcctctgcag 60


H: 231 gtgcgccgatgtccacagtgctaccttctgatgagctactgctttcattcagtttctgct 290
       ||||||||||||||||||||||||||||||| ||||||||||||||||| |||||||||||
R: 61  gtgcgccgatgtccacagtgctaccttctgaggagctactgctttcattcagtttctg-- 118
       | || || ||||| || ||||| || ||||| |||||||||||| || |||||||
M: 61  gcgccccaatgtctactgtgcttccctctgaggagctactgctttcgttgagtttct--- 117


H: 291 gacttaatatgtgagctgacagaatgcagagaccacgttgtatatgaagcatccactttg 350
                     ||||||||||||||||| |||||||||||||||||||||||||
R: 119 ----------------gacagaatgcagagaccacattgtatatgaagcatccactttg 161

M: 1   ----------------------------------------------------------


H: 351 ccttgtacaccagggcattcaataaccacttaataactacaaccctgatgatccgattca 410
       ||||||||| |||||||||||||||||||||||||||||||||||||||||||||||||||
R: 162 ccttgtacacaagggcattcaataaccacttaataactacaaccctgatgatccgattca 221
                          || | || ||| ||||| | ||||||||||||||| ||||||
M: 118 ------------------gatgatcagttactaactgcgaccctgatgatctgattca 158


H: 411 ctactaaagtcttccgtgtttaaattttcaaagtcagattctcctacagcaattggtaca 470
       |||||||||||||||||||||||||||||||||||||||||||||||||||||||||||||
R: 222 ctactaaagtcttccgtgtttaaattttcaaagtcagattctcctacagcaattggtaca 281
       || ||||||||| |||||| |||||| || |||||||||| ||||| ||||||| || |||
M: 159 ctgctaaagtcttctgtgtttaagttctcaaagtcagactctcccacagcaatgggcaca 219


H: 471 gtcacagtaagactggggttgtttatgaatgacatgtaatcactttcatcaataatgtat 530
       |||||||||||||||| ||||||||||||||||||||||||||||||||||||||||||||
R: 282 gtcacagtaagactgggattgtttatgaatgacatgtaatcactttcatcaataatgtac 341
       |||||||| ||||| || ||||||||||||||||||| ||||||||| |||||| |||||
M: 220 gtcacagtgaggctgggggttgtttatgaatgacatataatcactctcatcaatgatgtac 280
```

```
                       CUR-1740,CUR-1837
H:  531  ttttcaacactgctgccagttcctataccacttgtagttccatttacatctttaagatag  590
         |||||||||||||||||||||||||||||||||| ||||||||||||||||||||||||||
R:  342  ttttcaacactgctgccagttcctataccgcttgtagttccatttacatctttaagatag  401
         || || |||||||||| || ||||| |||||| |||||| |||||| || |||
M:  281  ttctccacactgctgcccgtccctatgccacttgtggttccattcacatctttcagacag  341
                       CUR-1901
H:  591  tcaagatctttcccaatttctgctgtatgattggacatacaactgtctttcttgttgttt  650
         |||||||||||||||||||||||| |||||||||||||||||||||||||||||||||||
R:  402  tcaagatctttcccaatttctgttgtatgattggacatacaactgtctttcttgttgttt  461
         || |||||||||||||||| ||| || |  || |||||| |||||||       ||
M:  342  tccagatctttcccaatttctgttgtgtggttagagatacaattgtcttttc------tt  396

H:  651  agatcatcaagtggtttaatttcatctaaaatcttttgtttcctaatgaaggactgttga  710
         |||||||||||||||||||||||||||||||||| |||| |||||||||||||||||||||
R:  462  agatcatcaagtggtttaatttcatctaaaatcttttgtttcctaatgaaggactgttga  521
         |||||||||||| |||  ||||||||||| |||| | ||||| |||  ||||| ||||||
M:  397  agatcatcaagtggcttaatttcatctagaatcttctgtttcttaacaaaggattgttga  457

H:  711  ataaattcatatatttttcttttcacataagctactcctttgtgcatcctatccacagca  770
         |||||||||| |||||||||||||||||||||||||||||||||||||||||||||||||
R:  522  ataaattcatatattttcttttcacataagctactcctttgtgcatcctatccacagca  581
         || |||||||||||||||||||||||| ||||||||||  ||||||||||||| |||||||
M:  458  atgaattcatatattttcttttacataagctattcctttgtgcatcctgtccacagca
                                               CUR-1924

H:  771  atttggagattattcatttcattatcatcatcagtggctgcaaggttgtctgcactaaat  830
         |||||||||| ||||||||||||||||||||||||||||||||||||||||||||||||||
R:  582  atttggagattgttcatttcattatcatcatcagtggctgcaaggttgtctgcactaaat  641
                  || ||||| |||| |||||||||||||||||||||||||||||||||||||
M:       ---------ttgttcatctcattgtcatcatcagtggctgcaaggttgtctgcactaaat

H:  831  gagctcagaagcaaggccagaaagagattcaggaccttaaaaacaacaaaaacatgatta  890
         ||||||||||||||||||||||||||||||||||||||| |||||||||||||
R:  642  gagctcagaagcaaggccagaaagagattcaggacctttaaaacaacaaaaacatgatta  701
         |||||||||||||||||||||||||||||| |||| ||||| ||||||
M:       gagctcagaagcaaggccagaaagaggttcaagaccttgaaaaca--------------

H:  891  taattttacaccaatgtagggaagagcagattacaatcacttattctttcttttaagtgt  950
         |||||||||| |||||||||||||||||||||||||||||||    ||||||| |||||
R:  702  taattttacaccgatgtagggaagagcagattacaatcactta----ttcttttcagtgt  757

M:       ------------------------------------------------------------

H:  951  ggaaaaaactctaagttctaaaacttgatgagaa**ggaaacaccacagcatagtgattag**a 1010
         |||| |||||||||||||||||||||||||||||||||||||||||||||||||||||||
R:  758  ggaagaaactctaagttctaaaacttgatgagaaggaaacaccacagcatagtgattaga  817

M:       ------------------------------------------------------------
            CUR-1916    CUR-1945
H: 1011  agat**ggg**tgatctgaatttgtgactggc*t*caatagcacatccttggacaaagacatgatt 1070
         ||||||||||||||||||||||||||||||||||||||||||| ||||||||||||||||
R:  818  agatgggtgatctgaatttgtgactggctcaatagcacatccctggacaaagacatgatt  877

M:       ------------------------------------------------------------

H: 1071  *tctgttgctctcaagttctcccattcgtaaagtgaaattgaatgagctaatct* 1123
         ||    ||||||||||||||||||||||| ||||||||||||||||||||||||
R:  878  tccattgctctcaagttctcccatttgtaaagtgaaattgaatgagctaatct 930

M:       ---------------------------------------------------
```

control article was loaded into a syringe coupled to a three-way stop-cock, the male port on which was attached to a 22 gauge 1.5 in. needle and the female port to another empty 1 cm³ polycarbonate Luer-lock syringe to apply negative pressure for controlled withdrawal of CSF to confirm entry into the CSF space. A second study participant then percutaneously introduced the needle into the cisterna magna by atraumatically gliding the needle tip down the poster aspect of the occipital bone to the foramen magnum. Two hundred and fifty milliliters of CSF was then slowly withdrawn over a 10–30 s interval, and the stop-cock turned to allow delivery of the test or control article, with

Fig. 2. Summary of AntagoNAT screening data. Bars show fold difference in the SCN1A mRNA expression levels between mock-transfected controls and cells treated with 20 nM of AntagoNATs of different chemistry and sequence. Boxes point to AntagoNATs selected for in-depth studies based on their high SCN1A upregulation and effect consistency in different cell lines. For mouse, homology to human AntagoNATs was also taken into account. Each bar represents an average of 2 or more experiments in 2 different cell lines (HepG2 and SK-N-AS cells for human, 3T3 and Neuro2a cells for mouse-specific AntagoNATs, $n = 10$ or higher). Real time PCR data. Mean $\pm$ S.E.M. $^* - p < 0.05$.

reintroduction of sufficient CSF to flush the test and control article from the catheter dead space. After successful needle withdrawal, the monkey was transferred to home cage. General animal well-being was assessed before, during and after sedation and anesthesia. A behavioral summary score was applied to evaluate treatment associated behavioral changes based on an objective, inter-rater reliable, quantitative rating of behavior by a well established protocol (Taylor et al., 1997). Behavior was observed twice at approximately the same time of day for a 5 min period prior to and after test article delivery. The total behavioral summary score (BSS) was derived from the summed activity measures at each observation time point, incorporating cumulative incidence per 5 second interval over the 5 minute observation period of the following healthy normal behaviors: shift, tail flag, yawn, chew, scratch, vocalization, self groom, cage pick, eating, drinking, threaten, lookout, lick fingers, cage lick, and vertical climb. Seven days after test or control article dosing the monkeys were euthanized with intravenous sodium pentobarbital followed by transcardial perfusion with chilled 0.9% saline for approximately 10 min to minimize residual intravascular blood and allow optimal sectioning of the brain. At the time of sacrifice animals were examined carefully for external abnormalities including hair loss, palpable masses, and abnormalities in the abdominal and thoracic cavities. Brain, spinal cord, heart, lung, liver, spleen, and kidney specimens were dissected and punch biopsies obtained and flash frozen for

bioanalytical and pharmacodynamic analyses. The remaining harvested CNS tissue was post-fixed in 4% paraformaldehyde, then transferred to PBS with 0.05% azide and retained for histological analysis. Brain tissue processing and histopathological analysis was conducted by HistoTox Labs Inc. (Boulder, CO).

2.14. AntagoNAT Detection In Situ

Formalin fixed monkey brain specimens were paraffin-embedded and sectioned into 8 μm slices that were then adhered onto charged glass slides. To perform Fluorescent In Situ Hybridization (FISH), the slides were heated at 70 °C for 30 min, deparaffinized by passing through a xylene and ethanol series, microwaved in 10 mM citrate buffer for antigen retrieval and washed in PBS. The tissue slides were incubated in a pre-hybridization buffer (3% BSA in saline-sodium citrate (SSC)) at 65 °C followed by treatment with the AntagoNAT-specific LNA probe labeled with TYE™ 563 (TYE™ 563/+G + GG + TG + AT + -CTG + AA + TT + TGT + GAC + TG, where + designates an LNA modification) denatured for 5 min at 75 °C and dissolved in hybridization buffer (10% Dextran Sulfate in SSC), for 1 h at 65 °C. After probe annealing, the slides were extensively washed in wash buffers (SSC and PBS). The slides were blocked in donkey serum then incubated with primary antibody for parvalbumin (R&D Systems, USA) overnight at 4 °C,

Table 2
SCN1ANAT sequence conservation.[a]

	Score	Length	Identity, %	Chromosome	Locus	Start	End
Chimpanzee	1097	1115	99.3	2B	Scn1a	8	1123
Orangutan	1058	1116	97.7	2b	Scn1a	7	1123
Gorilla	1035	1058	99.2	2B	Scn1a	65	1123
Rhesus	886	952	97.7	12	Scn1a	171	1123
Marmoset	855	952	95.0	6	Scn1a	171	1123
Pig	541	752	91.4	15	Scn1a	339	1091
Mouse	371	475	89.1	2	Scn1a	400	875
Chicken	290	444	82.1	7	Scn1a	405	849
Zebrafish	40	280	97.7	11	n/a	523	803
C. elegans	20	25	88.5	I	n/a	786	811

[a] Identity to human. Columns LENGTH and IDENTITY refer to the regions of high homology only. Columns START and END show positions on SCN1ANAT. Total length of human SCN1ANAT is 1123 nucleotides.
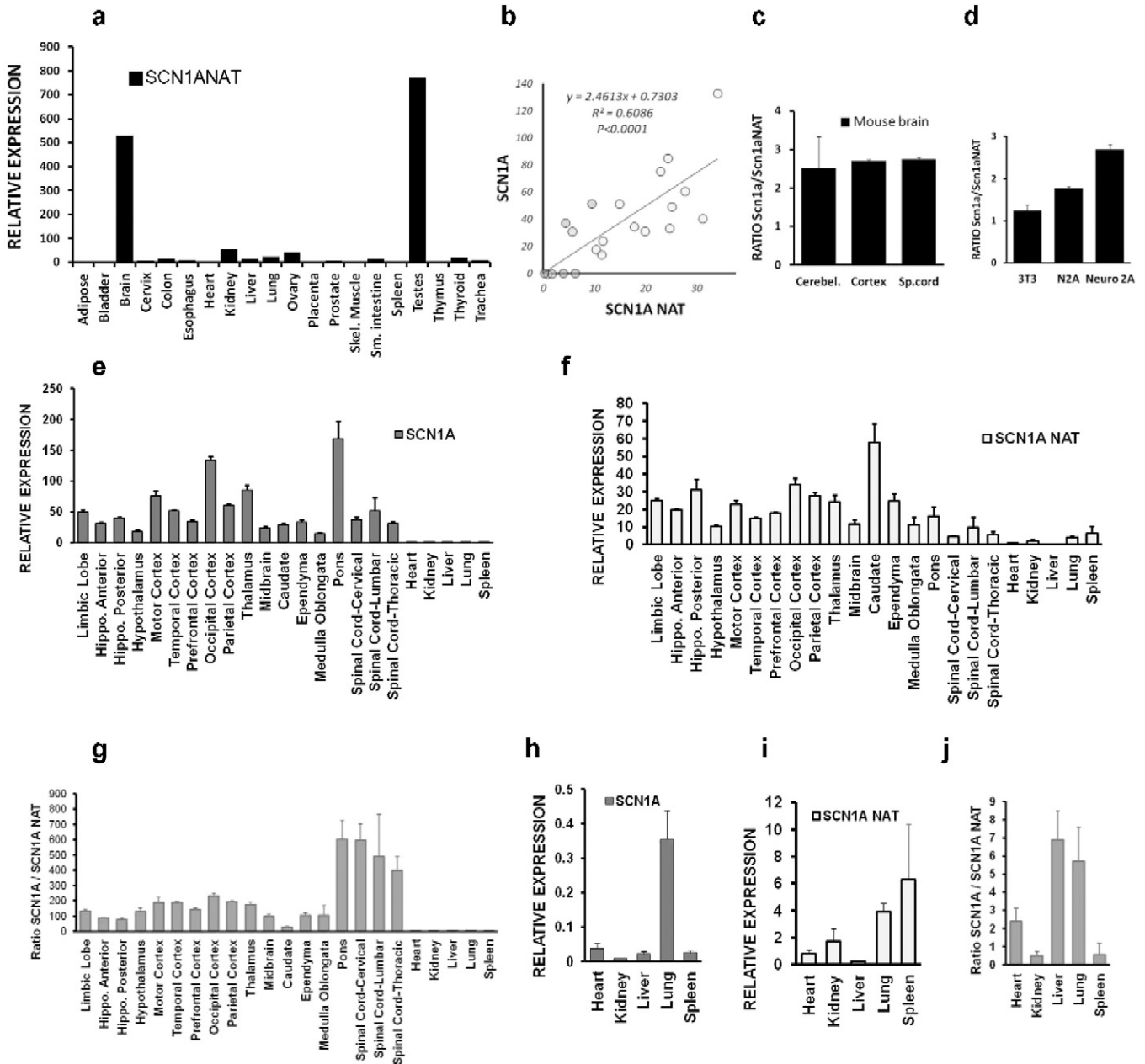
Fig. 3. SCN1A and SCN1ANAT expression in human, monkey and mouse tissues. (a) Expression of SCN1ANAT in a human tissue panel, normalized to arbitrary RNA standard. (b) Correlation of expression levels of Scn1a and Scn1aNAT in African green monkey tissues ($n = 4$, df $= 20$, F $= 29.5$; tissues as listed in (e), dark circles — peripheral organs, lighter circles — spinal cord, light circles — brain regions). (c) Ratio of Scn1a to Scn1aNAT expression in mouse tissues, $n = 4$. (d) Ratio of Scn1a to Scn1aNAT expression in mouse cell lines. (e–g) Expression levels of Scn1a and Scn1aNAT in African green monkey tissues, $n = 4$: (e) — Scn1a mRNA. (f) — Scn1aNAT RNA. (g) — Ratios of Scn1a to Scn1aNAT copy numbers. (h–j) — Enlarged portions of e, f, g respectively showing data for peripheral organs. Real time PCR data. Mean ± S.E.M.

followed by secondary antibody (donkey anti-sheep, labeled with Alexa 488 (Jackson ImmunoResearch, USA) diluted 1:250 in PBS for 1 h at 37 °C. Lastly, the slides were washed again with PBS and cover slipped in Vectashield mounting media with DAPI (Vector Laboratories).

2.15. Hybridization Assay

A hybridization assay was developed to determine concentrations of the AntagoNAT CUR-1916 in biological samples from animal studies including plasma, CSF, brain and peripheral organ tissues. Briefly, we designed 2 probes to specifically detect CUR-1916: a capture probe (5AmMC12//iSp18//iSp18/ G*G*G*+T*+G*+A*+T*+C*+T*+G*+A*+A*+T where * designates a phosphorothioate bond, + designates LNA modification, 5AmMC12

is 5′-amino modifier C12m, Sp18 is an internal 18-mer spacer) and a detection probe (+T*+G*+A*+C*+T*+G*+G*+C*+T*+C/iSp18// iSp18//iBiodT//3BioTEG, where iBiodT is an internal biotin-dT, 3BioTEG is a 3′ biotin-TEG, all manufactured by IDT Inc.). DNA-Bind plates were incubated with capture probes overnight, then blocked with bovine serum albumin for 2 h. Biological samples were mixed with detection probes in a sample preparation plate and heated at 90 °C for 12.5 min. The detection probes/sample mixtures were then transferred to the capture plate and incubate at 45 °C for 2 h. The plate was incubated with Streptavidin HRP for 30 min followed by TMB substrate for 30 min in the dark. The reaction was stopped with sulfuric acid. Absorbance was measured using a spectrophotometer at 450 nm with background correction set to 650 nm. The hybridization method was validated using known amounts of AntagoNAT added to brain tissue
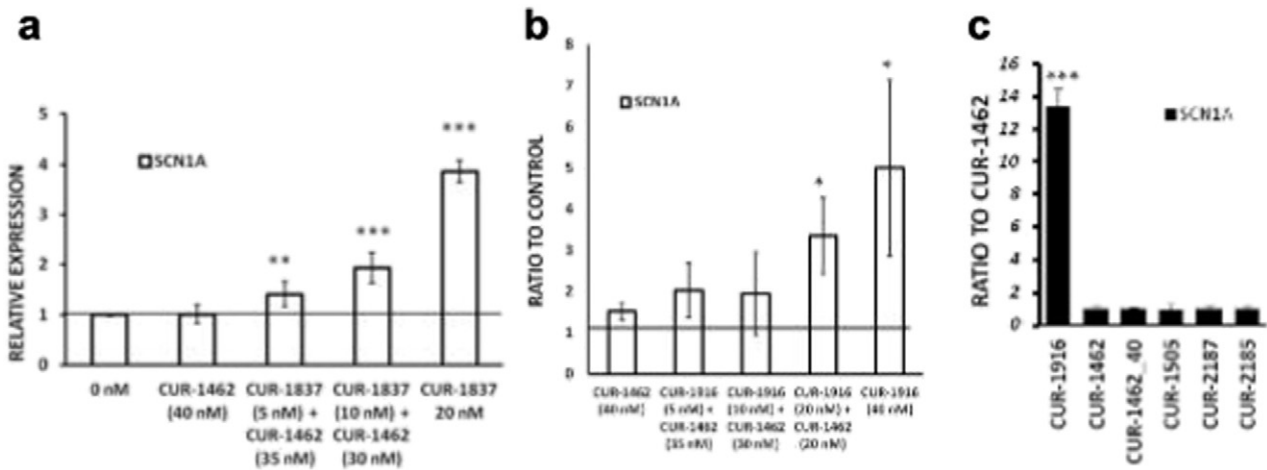
Fig. 4. Target specificity of NAT-mediated SCN1A upregulation. (a) SCN1A mRNA in SK-N-AS cells treated with a mixture of active AntagoNAT (CUR-1837) and a control oligonucleotide (CUR-1462); ANOVA $p < 0.01$, $n = 3$–5. (b) Vero76 cells treated with a mixture of an active AntagoNAT (CUR-1916) and control oligonucleotide (CUR-1462); ANOVA $p < 0.05$, $n = 5$/group, representative of 4 experiments. (c) SCN1A mRNA levels in SK-N-AS cells treated with 20 nM of an active AntagoNAT (CUR-1916) or inactive oligonucleotides of different sequence and chemistry (except CUR-1462_40 at 40 nM; ANOVA $p < 0.001$, $n = 6$/group, representative of 11 experiments). Real time PCR data. Mean ± S.E.M., * − $p < 0.05$, ** − $p < 0.01$, *** − $p < 0.001$.

extracts from untreated monkeys. Validation of the method included specificity/dilution linearity, working calibration range, lower limit of quantitation and intra-assay precision and accuracy. The lower limit of quantitation was determined to be 0.4 ng/ml, and the back-calculated concentrations of the calibration standards were within ± 20% of their theoretical concentrations over the working range of 0.4 to 10 ng/ml using a 4-parameter logistic curve fit (SoftMax PRO, Version 5.4.1, Molecular Devices Corporation). Intra-assay accuracy was within ± 20% of the nominal concentrations (± 25% for the lower limit of quantitation) and precision was within 20%. Samples of monkey brain lysate containing AntagoNAT were shown to be stable in at room temperature for over 4 h and after four freeze-thaw cycles at approximately − 20 °C. The molar concentration of AntagoNAT in the tissue can be calculated by

dividing the detected amount of AntagoNAT by its molar mass (8566.9 g/mol). For example, AntagoNAT concentrations in the CSF seven days after injection were 5.27 ± 1.99 ng/ml (or 0.615 nM) at the 0.008 mg/kg dose and 16.79 ± 4.12 ng/ml (or 1.96 nM) at 0.04 mg/kg ($n = 6$).

2.16. Statistical Analysis

Data was analyzed using Excel except where noted. *t*-Tests were used when 2 groups were compared, one-factor ANOVAs when comparing a single factor in >2 groups, two-factor ANOVAs were used to compare more than one factor in >2 groups, (both ANOVAs with custom Tukey post-hoc test), *t*-test with Bonferroni correction was used when 2
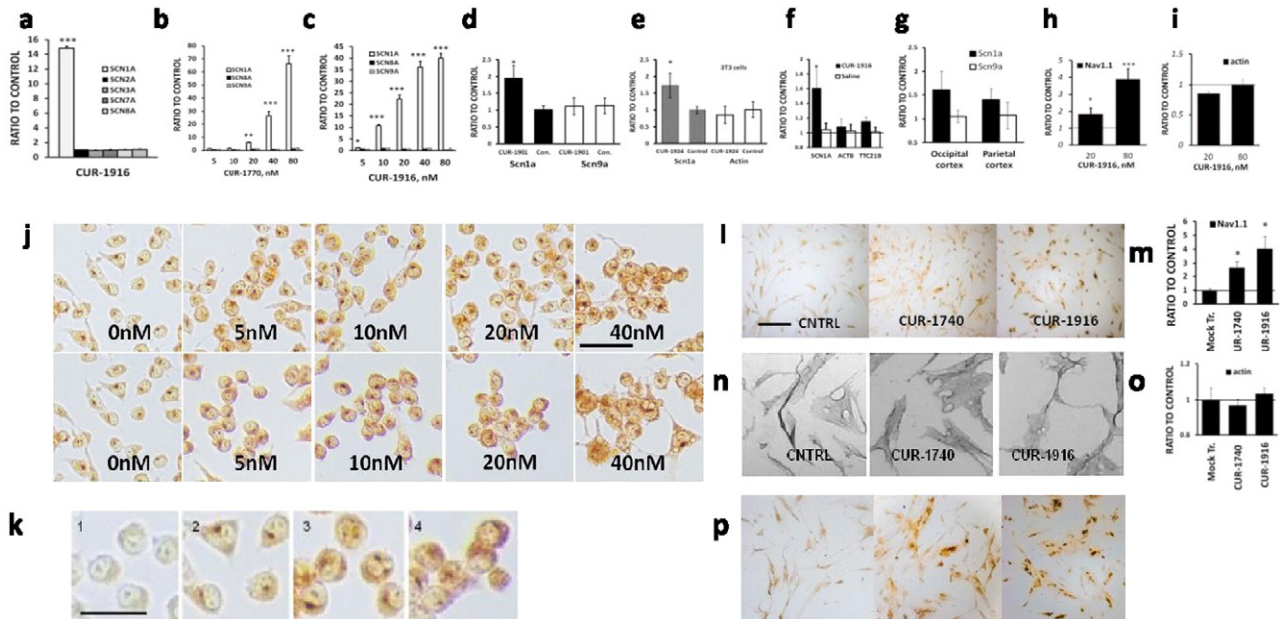
Fig. 5. Treatment with AntagoNATs did not affect expression of highly homologous alpha subunits of sodium channels and unrelated genes. (a) Human SK-N-AS cells, 20 nM CUR-1916 ($n = 5$, $p < 0.001$ for Scn1a). (b, c) Dravet patient fibroblasts D-00 treated with different concentrations of (b) CUR-1770 or (c) CUR-1916; real time PCR data, ANOVA, $p < 0.05$ for SCN1A, $p > 0.05$ for other genes, $n = 5$/group. (d, e) mouse 3T3 cells ($n = 10$/group, $p < 0.02$ for Scn1a), (f) monkey temporal cortex *in vivo* ($n = 9$, $p < 0.01$ for Scn1a), (g) Dravet mouse brain *in vivo* ($n = 9$, $p < 0.01$ for Scn1a, *t*-test with Bonferroni correction, $p > 0.3$ for all other genes). (h, i) Protein levels in Vero76 cells after treatment with CUR-1916: (h) Nav1.1 and (i) actin (ELISA, $n = 3$, 1-factor ANOVA $p > 0.05$ for actin, $p < 0.05$ for Scn1a). (j) IHC staining for Nav1.1 after treatment of Neuro2a cells with CUR-1901 (top panel and CUR-1924 (bottom), (k) magnification of (j), 1 − no primary antibody, 2–0 nM, 3.4–40 nM of CUR-1901 or CUR-1924 respectively. (l–p) − Treatment of Dravet fibroblasts with 80 nM of AntagoNATs upregulates Nav1.1 (l, m, p) but not actin (n, o) protein levels (IHC staining, NIS-ElementsD3.0 software, $n = 4$, 2-factor ANOVA $p < 0.05$ for actin, $p < 0.05$ for Scn1a). Mean ± S.E.M., * − $p < 0.05$, ** − $p < 0.01$, *** − $p < 0.001$.
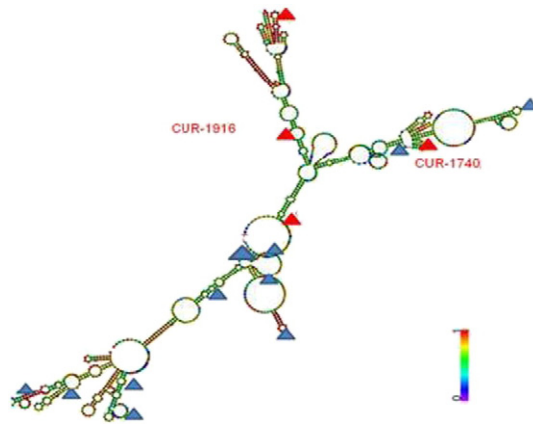
Fig. 6. Secondary structure of SCN1ANAT. Blue triangles — low-activity, red triangles — high-activity AntagoNAT clusters. AntagoNATs inducing highest upregulation of SCN1A were located around positions 540 and 1018 (representative AntagoNATs CUR-1740 and CUR-1916 respectively). Color scale represents probability of occurrence of the secondary structure (blue — low, red — high). Generated using Vienna RNAfold software.

groups were compared on several factors, linear regression was used to confirm an increase/decrease trend in one factor depending on another, and multiple regression was used to estimate the degree and probability of determination of one factor by multiple other factors. Excel F-test tool and QQplots, respectively, were used to compare sample variances and estimate normality. Fisher exact test was used to compare frequencies by an on-line calculator (Preacher and Briggs, 2001). Statistical analysis of RNAseq results is described in corresponding section. Group size determination was conducted using custom calculator. Sample size in all studies was calculated assuming alpha of 0.05 and power of 0.80 using standard deviation values estimated in pilot experiments. All tests were 2-sided. Criteria for data exclusion were defined for each analytical technique in lab SOPs at the time of method validation experiments. Scientists carrying out animal treatment and analytical tests were blinded to group assignments. Analytical tests, animal treatment and data analysis were carried out by independent groups of scientists. All data is presented as mean ± S.E.M., group size is indicated in figure legends or on the graphs.

3. Results

3.1. SCN1A Locus is Regulated by NATs in Different Species

In the NCBI transcript database we identified an RNA transcript expressed from the opposite DNA strand of the human SCN1A locus that we named SCN1ANAT (accession number BG724147, Fig. 1a). We then sequenced the complete insert of the BG724147 cDNA clone, extending SCN1ANAT to 1123 nucleotides. Seven additional sequences in

the NCBI database closely homologous to BG724147 have been cloned from several tissues by different authors. To better define the boundaries of SCN1ANAT we performed 3′ and 5′-RACE experiments using RNA from Dravet fibroblasts, testes and HepG2 cells, which confirmed the 3′-end of SCN1ANAT (Table 1).

To study the potential regulatory effects of this ncRNA on SCN1A expression, we designed >70 oligonucleotide-based compounds, termed AntagoNATs, targeting different regions of SCN1ANAT, and transfected them in several cell lines. In these experiments 86% of the AntagoNATs induced an increase in SCN1A mRNA levels at the initial screening concentration of 20 nM, suggesting that SCN1ANAT acts as a negative regulator of SCN1A expression (Fig. 2).

The Scn1aNAT sequences are highly conserved in primates, but have only limited homology in pig, mouse and chicken (Table 2). Notably, in these species small regions of homology to SCN1ANAT map to the Scn1a loci, supporting functional conservation. Examination of mouse databases yielded two potential Scn1aNAT sequences. We focused on the Scn1aNAT1 (Fig. 1b) because its position relative to the Scn1a coding regions was similar to human SCN1ANAT. We then designed 36 mouse-specific AntagoNATs and showed that >80% of them induced Scn1a upregulation in 4 mouse cell lines, thus confirming the conserved regulatory activity of Scn1aNAT1 in repressing Scn1a expression (Fig. 2).

3.2. SCN1ANAT is Expressed in Multiple Tissues

SCN1A is normally expressed in multiple excitable and non-excitable cells, reflecting its roles in generating action potentials and maintenance of cellular homeostasis (GNF Expression Atlas 2; The Human
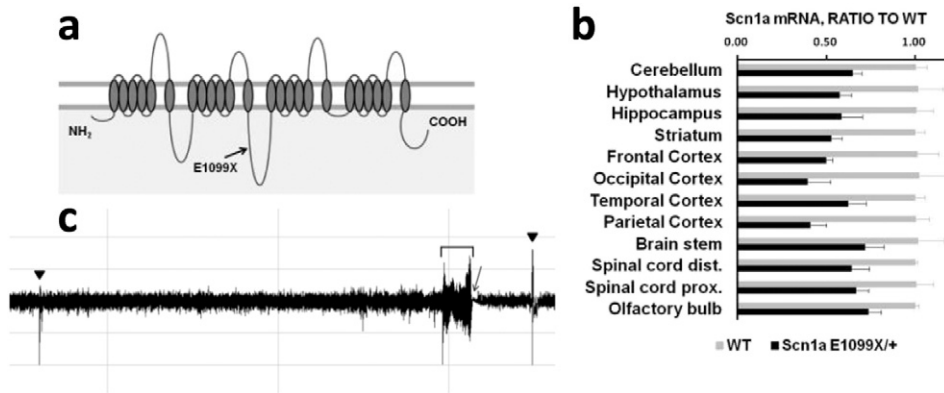
Fig. 7. Mouse model of Dravet syndrome. (a) Localization of the E1099X mutation in the Scn1a protein structure. (b) Scn1a mRNA expression in Scn1a E1099X/+ mice compared to WT, real time PCR data, $n = 3$. (c) Example of a 12-hour long EEG recording showing typical seizure (square bracket), post-seizure depression (slim arrow) and inter-ictal activity (block arrows); representative of the 28-day continuous observation of >30 mice (video in Supplementary File 3). Mean ± S.E.M.
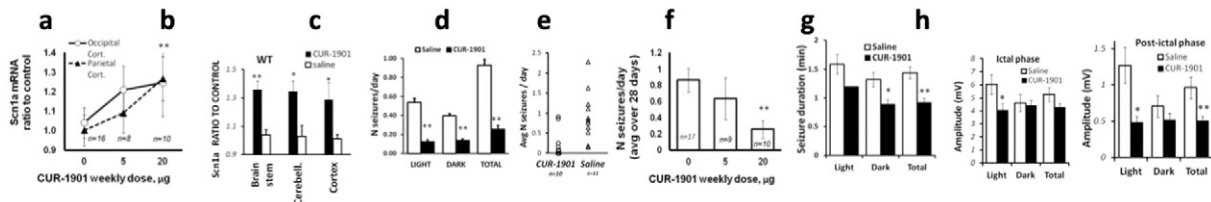
Fig. 8. SCN1A upregulation and seizure phenotype improvement in a mouse model of Dravet syndrome after AntagoNAT treatment in vivo. Mice were treated with 4 weekly injections of CUR-1901 at 20 μg/injection or saline. (a, b) Dose-dependent increase in Scn1a mRNA levels in brain regions of Scn1a E1099X/+ (a) or WT (b) mice (real time PCR data, normalized to vehicle control, ANOVA $p < 0.05$ for each brain region, stars show comparison to 0 μg). (c) Average number of seizures recorded during the 12 h light (LIGHT) or dark (DARK) periods, and TOTAL throughout the day (average over 28 days; $n = 10$ for CUR-1901, $n = 11$ for control, t-test with Bonferroni correction). (d) Total number of seizures from (a), symbols represent averages for individual animals. (e) Dose-dependent reduction in daily seizure numbers (regression $p = 0.01$). (g–i) Reduction in (g) seizure duration, (h) ictal amplitude and (i) post-ictal amplitude ($n = 6$ for CUR-1901, $n = 5$ for saline, t-test with Bonferroni correction). Mean ± S.E.M. * − $p < 0.05$, ** − $p < 0.01$.

Protein Atlas). However, SCN1A expression in non-neuronal tissues and cultured cells is 10–1000 times lower than in the CNS. Correspondingly, SCN1ANAT expression was also observed in all human, monkey and mouse tissues tested, with highest levels in the brain and testes (Fig. 3a, f, i). In order to estimate the average level of SCN1ANAT (AC010127.3) in cells we analyzed data from the Developmental Transcriptome project of the BrainSpan Atlas. This project consists of RNAseq data profiling up to 16 cortical and subcortical regions across 13 developmental stages. One copy of a transcript per cell corresponds to reads per kilo base per million mapped reads (RPKM) values between 0.5 and 5, depending on the total amount of RNA per cell (Mortazavi et al., 2008). In the BrainSpan data the average RPKM value for SCN1ANAT is 1.28, corresponding to approximately one transcript of SCN1ANAT per cell. The SCN1A/SCN1ANAT ratio in a pooled sample of 3 human brains was comparable to the average African green monkey brain ratio (64.7 ± 8.5 and 138 ± 58, respectively), while the ratio in the mouse CNS was significantly lower (2.6 ± 0.7, Fig. 3). Scn1aNAT expression positively correlated with Scn1a mRNA expression in most monkey tissues ($r^2 = 0.61$, $p < 0.001$; Fig. 3b). The positive correlation between SCN1A and SCN1ANAT expression could reflect the need for a larger pool of replacement NAT molecules in more active loci due to higher probability of NAT molecule damage or displacement.

3.3. Effects of Blocking SCN1ANAT are Highly Gene-specific

We then investigated if the increase in transcription induced by blocking SCN1ANAT is specific to the SCN1A gene. In the first set of experiments, an inactive control oligonucleotide with no homology in the human genome was added to an active AntagoNAT of similar chemistry to keep the combined oligonucleotide concentration constant. After treatment of SK-N-AS cells with this oligonucleotide mix, SCN1A mRNA levels increased proportionally to the dose of the active AntagoNATs, but not the control oligonucleotide or total chemistry load (Fig. 4a). We repeated this experiment using different AntagoNATs and cell lines and observed that SCN1A upregulation was not associated with a particular AntagoNAT sequence, chemistry or cell line (Fig. 4b), indicating that the effect was target-dependent. Similar effect was observed at the protein level (Fig. 5j–p). SCN1A levels in cells treated with inactive oligonucleotides did not differ from mock-transfected controls (Fig. 4c).

In the second set of experiments we showed that treatment with AntagoNATs targeted against SCN1ANAT did not affect the expression of other alpha subunits of sodium channels, which are highly homologous to SCN1A (SCN2A, SCN3A, SCN9A, SCN7A, SCN8A) and of unrelated genes, localized either next to SCN1A on chromosome 2 (Ttc21b) or on a different chromosome (actin). The absence of effect was observed in human and mouse cell lines (Fig. 5a–e) and in vivo in African green monkeys and Dravet mice (Fig. 5f–g). Expression of the studied genes in cells treated with inactive oligonucleotides was not different from mock-transfection or vehicle controls.

In the third set of experiments we performed high throughput RNA sequencing (RNAseq) to compare the transcriptomes of SK-N-AS cells

treated with either an active AntagoNAT (CUR-1916) or an inactive control oligonucleotide of similar chemistry (CUR-1462). Sequencing generated a minimum of 76,000,000 passed-filter-paired-end reads per sample, which aligned to the reference genome at an average 83% ± 0.5% efficiency and mapped to >31.000 genes (Supplementary File 1). Differential expression analysis showed that 90.3% of the expressed genes did not differ between cells treated with the active and control AntagoNATs. Similarly to what we observed using real time PCR, RNAseq results showed that SCN1A levels in the active AntagoNAT-treated samples were upregulated 4.2 fold compared to control ($p < 0.0001$, FDR = 0.00001). Expression of other sodium channel genes (SCN2A, SCN3A, SCN5A SCN7A, SCN8A, SCN9A, SCN1B, SCN3B), as well as genes flanking SCN1A on chromosome 2 (TTC21B and SCN9A) did not differ between the two groups (Supplementary File 1). Of the 9.7% of genes with significant changes in expression, 56% represented non-coding RNA (pseudogenes, lincRNA, miRNA, NATs, rRNA, snRNA, and other types) with little or no information on their function. The remaining 44% were protein-coding genes. Among protein coding genes, 28% had no known function (Supplementary File 2). Based on the information about the remaining 72% of the differentially expressed protein-coding genes obtained from different annotation tools, they could be divided into 2 major groups: 1) housekeeping genes needed to support increased RNA and protein expression (57%), and 2) genes involved in neuronal and astrocytic differentiation (43%, Supplementary File 2). The increased expression of these genes could occur as a downstream effect of the AntagoNAT-mediated increase of SCN1A expression. SK-N-AS is a human neuroblastoma cell line, which represents a mixed population of cells resembling early neuronal and glial phenotypes (Thiele, 1998). SK-N-AS cells are known to differentiate spontaneously or under external stimuli, including overexpression of certain genes (e.g. TRKB, RET), giving rise to a mix of neuronal- and glial-like cells (Thiele, 1998). Interestingly, in active AntagoNAT-treated samples expression of anticonvulsant neuropeptides and their receptors, including neuropeptide FF (NPFF), neuropeptide FF receptor 2 (NPFFR2), galanin receptor 2 (GALR2) and ghrelin/obestatin prepropeptide (GHRL), was upregulated or likely upregulated compared to controls (Supplementary File 1).

Taken together, the results from the 3 sets of experiments indicate that SCN1ANAT-mediated increase of SCN1A expression does not result from spurious qualities of one AntagoNAT, non-specific chemistry effect, generalized transcriptional upregulation or class effect involving all sodium channels. In addition, it is restricted to genomic SCN1A locus, while the expression of highly homologous and adjacent genes, and of >90% of all expressed genes, remains unchanged.

3.4. Secondary Structure of SCN1ANAT Determines the Degree of AntagoNAT Effect

While 86% of AntagoNATs designed against SCN1ANAT induced SCN1A upregulation at 20 nM, the scale of upregulation was different (Fig. 2). One possible reason for these differences is the localization of

Table 3
Multiple regression of seizure numbers on Scn1a levels in different brain regions of Scn1a$^{E1099X/+}$ mice.[a]

Regression statistics					
Multiple R					0.815
R squared					0.664
Adjusted R squared					0.472
Standard error					0.487
Observations					23

ANOVA					
	df	SS	MS	F	Significance F
Regression	8	6.546871646	0.818	3.455711	0.020648545
Residual	14	3.315388717	0.237		
Total	22	9.862260363			

	Coefficients	Standard error	t stat	p-Value
Intercept	−2.71	1.516	−1.79	0.0951
Cerebellum	1.09	1.006	1.085	0.2962
Hypothalamus	0.70	0.772	0.905	0.3807
Hippocampus	2.55	0.968	2.633	0.0197
Striatum	−0.14	0.590	−0.233	0.8190
Frontal cortex	1.08	0.978	1.107	0.2869
Occipital cortex	−1.12	0.485	−2.316	0.0362
Temporal cortex	0.50	0.569	0.871	0.3983
Parietal cortex	−1.12	0.431	−2.603	0.0208

[a] Scn1a$^{E1099X/+}$ mice were continuously EEG- and video-monitored for a 28-day period starting at postnatal week 7, after which SCN1A mRNA levels in regions covering the whole brain were determined by real time PCR. Multiple regression on this data shows that 66% of the variation in seizure frequency could be explained by differences in Scn1a levels ($p = 0.02$; $n = 23$). Scn1a levels in a subset of brain regions significantly correlated with the number of seizures.

AntagoNAT target sequence relative to the 3D structure of SCN1ANAT. To test this hypothesis, we designed a set of 19- to 21-base AntagoNATs covering full human SCN1ANAT sequence. When their ability to up-regulate SCN1A in different cell lines was compared, AntagoNATs complementary to sequences around positions 540 and 1018 of SCN1ANAT had the highest activity. In the model generated using Vienna RNAfold software (Gruber et al., 2008), these regions folded together into the same area of the SCN1ANAT secondary structure (Fig. 6). We confirmed these findings using two algorithms available in RNAfold, as well as in the Moscow University RNA Secondary Structure Prediction Tool, with highly similar results. These 'hotspot' regions may be essential for SCN1ANAT folding and function and/or be easily accessible to AntagoNATs.

3.5. Transgenic Mouse Carrying a Dravet Mutation Closely Mimics Human Disease

To test whether Scn1a upregulation after birth would lead to an improvement of disease symptoms *in vivo*, we injected AntagoNATs in transgenic mice harboring a known Dravet mutation E1099X (Fig. 7a), created in the laboratory of Dr. S.W. Lin (Tsai et al., 2015). The Scn1a$^{E1099X/+}$ model closely resembled previously described knockout and knock-in models of Dravet (Yu et al., 2006; Ogiwara et al., 2007; Oakley et al., 2011; Yamakawa, 2011, Kalume et al., 2013; Liautard et al., 2013, Martin et al., 2010) which share the major phenotypic features of the syndrome, including reduced Scn1a expression, seizure onset in early development, increased susceptibility to heat induced seizures, increased mortality with a sharp peak in early development, and reduced interneuron excitability. In Scn1a$^{E1099X/+}$ heterozygous mice, Scn1a mRNA levels in most brain regions were approximately 50% of wild-type (WT) controls (Fig. 7b). When continuously EEG-monitored from postnatal week (PW) 7 to PW11, approximately 80% of the Scn1a-$^{E1099X/+}$ mice demonstrated spontaneous seizures with the frequency of 0.9 ± 0.2 per day. Example of an EEG recording of a typical seizure episode with post-ictal EEG suppression, frequently observed in Dravet (Kim et al., 2014), is shown in Fig. 7c, video in Supplementary File 3. Seizures occurred during light and dark periods of the day with equal frequency (Fig. 8). Heat-induced seizure thresholds of Scn1a$^{E1099X/+}$ mice were significantly lower than those of WT mice (see data below). Similar to Dravet patients and other mouse models, high death rate was observed during a short period in early development (PW3–5 in case of the Scn1a$^{E1099X/+}$ mice), after which mortality
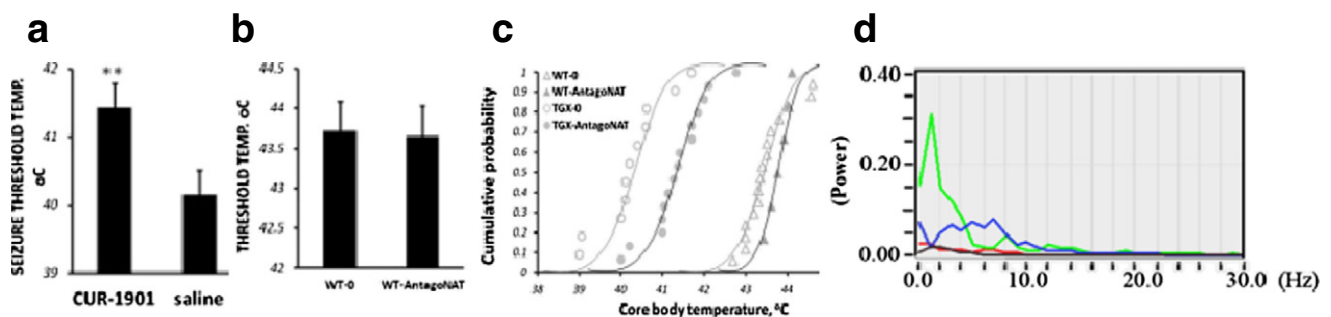
Fig. 9. Increase in seizure threshold temperature after CUR-1901 treatment. Scn1a E1099X/+ (a) or WT (b) mice were treated with 4 weekly injections of CUR-1901 at 20 µg/injection or saline. ($n = 4.6$, representative of 3 experiments, t-test $p = 0.01$). (c) Cumulative seizure probability vs core body temperature for WT and Scn1aE1099X/+ transgenic mice treated with CUR-1901 or vehicle ($n = 3.3,6,5$ respectively, representative of 3 experiments). (d) Power spectra of normal EEG (red trace), inter-ictal EEG (green trace), ictal EEG (blue trace) and post-ictal suppression EEG (black trace) in Scn1aE1099X/+ transgenic mice ($n = 6$).Mean ± S.E.M. ** − $p < 0.01$.
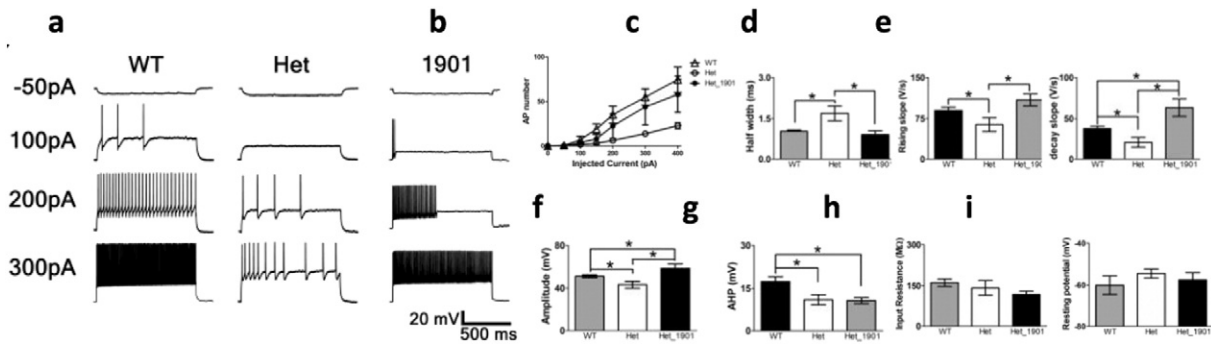
Fig. 10. Normalization of neuronal activity in Dravet mice after CUR-1901 treatment. WT and Scn1a E1099X/+ mice were treated with a single IT injection of 5 µg of CUR-1901 or saline. (a) Representative traces of current clamp experiments in hippocampal parvalbumin-positive interneuron in WT and control Scn1a E1099X/+ mice (Het), compared to Scn1a E1099X/+ treated (Het_1901) mice. (b) Input/output function for (a). (c–i) Characteristics of hippocampal parvalbumin-positive neurons ($n = 6.5.8$ respectively): (c) half-width of action potential (AP); (d) rise slope of AP; (e) decay slope of AP; (f) amplitude of AP; (g) afterhyperpolarization (AHP) amplitude of AP; (h) input resistance; (i) resting potential (t-test with correction, $p > 0.05$). Mean ± S.E.M., * − $p < 0.05$, ** − $p < 0.01$.

decreased. In particular, 48.2% of heterozygous mice survived to PW5, 33.4% to PW7, and 31.9% to PW10, while in WT mice 97% survived to PW10. The peak in mortality observed in Dravet mice may be related to the developmentally regulated decrease in Scn3a coinciding with increase in Scn1a expression (Cheah et al., 2013). Compared to WT, the Scn1aE1099X/+ mice had reduced interneuron excitability and altered action potential characteristics (see data below).

3.6. Increasing Scn1a in Adult Dravet Mice Improves Spontaneous Seizure Phenotype

To study the effects of SCN1A upregulation, seven week old Scn1a-E1099X/+ mice were injected intrathecally (IT) in the lumbar spine with different doses (5 and 20 µg) of a mouse-specific AntagoNAT CUR-1901, once weekly for 4 weeks. Mice were monitored by EEG and video recording 24 h a day continuously throughout the 28-day treatment period. Frequency and severity of seizures was assessed using combined EEG and video recording data. After the 4-week treatment with CUR-1901 or saline, a dose-dependent increase of 10–30% in Scn1a mRNA levels was observed in the brain of AntagoNAT-treated Scn1aE1099X/+ mice compared to control ($n = 16$ for control, $n = 8.10$ for CUR-1901, ANOVA $p = 0.05$, Fig. 8a). A similar upregulation of Scn1a was observed in AntagoNAT-treated WT mice (Fig. 8b). Furthermore, AntagoNAT treatment was associated with dose-dependent decline in average seizure number in Dravet mice (70% at 20 µg/injection, Fig. 8c–e). The average number of seizures in vehicle-treated mice over this period was 0.93/day (ranging from 0.15/day to 2.29/day). In mice treated with 20 µg/injection of AntagoNAT it was 0.26/day (ranging from 0/day to 0.92/day, Fig. 8d). Seizure number was equally reduced during light and dark periods of the day ($n = 10$/

group, t-test $p < 0.05$, Fig. 8c). The duration of the few seizures that occurred in AntagoNAT-treated animals during treatment week 4 was significantly decreased (Fig. 8f). The amplitude of ictal and post-ictal phases during the light periods was significantly decreased in CUR-1901-treated mice compared to controls, and a downward trend was observed during dark periods ($n = 5$ in AntagoNAT-treated group, $n = 6$ in control, $p < 0.05$, Fig. 8g, h). Amplitude reduction in post-ictal state may be due to neuropeptide-induced decrease in neuronal excitability (see RNAseq data above). By treatment week four, 50% of seizures in AntagoNAT-treated mice and 36% of seizures in saline-treated mice were below stage 5, however this difference was not statistically significant (Fisher exact test $p = 0.305$). Importantly, multiple-regression analysis of data from Scn1aE1099X/+ mice showed that 66% of the variation in seizure frequency could be explained by differences in Scn1a levels ($p = 0.02$; $n = 23$; Table 3). The finding of positive and negative correlations between seizure number and Scn1a levels in different brain regions including hippocampus, occipital and parietal cortices, is consistent with the network-based mechanism of seizure generation in Dravet and likely reflects the important but differential roles played by these regions in seizure generation. WT mice treated with an active AntagoNAT or saline vehicle did not show any behavioral manifestations of seizures.

Taken together, these experiments demonstrated that AntagoNAT-mediated increase of Scn1a in adult Dravet mice (Scn1aE1099X/+) can improve spontaneous seizure phenotype.

3.7. Upregulation of Scn1a Reduces Sensitivity to Heat-induced Seizures

Fever-induced seizures are frequently the first manifestation of Dravet syndrome. Correspondingly, in Scn1aE1099X/+ mice heat-induced

Table 4
Properties of hippocampal parvalbumin-positive interneurons (PVINs).[a]

Parameter	WT	Scn1a^E1099X/+	CUR-1901-treated Scn1a^E1099X/+
Input resistance (MΩ)	161.2 ± 13.7	141.7 ± 27.4	117.2 ± 12.6
Resting potential (mV)	−60.12 ± 4.5	−54.49 ± 2.2	−57.62 ± 3.6
Half width (ms)	1 ± 0.05	1.7 ± 0.27	0.9 ± 0.14

[a] Data from dentate gyrus PVINs of WT ($n = 7$), Scn1a^E1099X/+ ($n = 5$), 1901-treated Scn1a^E1099X/+ ($n = 8$) mice.

Table 5
SCN1A mutation types in cultured Dravet fibroblasts.

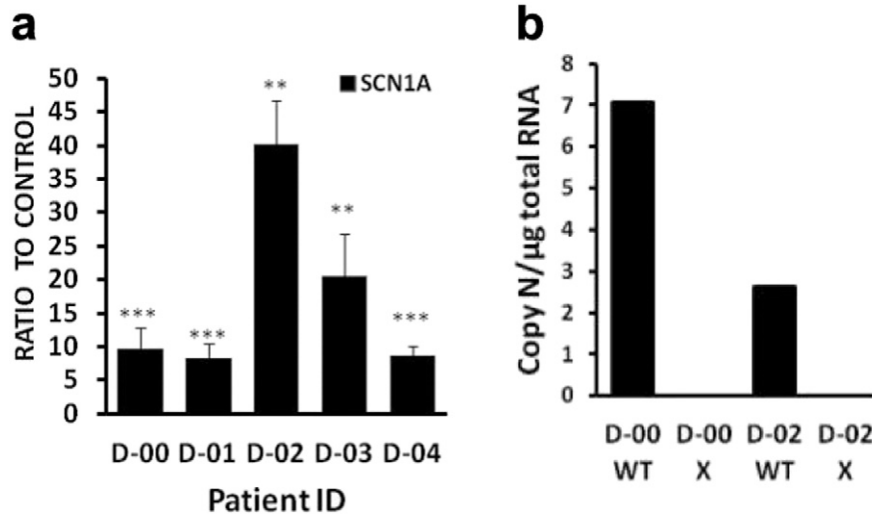| Patient ID	Mutation type
10	Codon change GAAtoTAA (glutamate to stop) at residue 1099
D-01	Codon change CtoT (threonine to isoleucine) at residue 367
D-02	Deletion T at position 1209 (frame shift)
D-03	Codon change TtoG (leucine to arginine) at residue 1359
D-04	Duplication (cgacacgg) at positions 1844–1845 (truncated protein)

Fig. 11. Upregulation of SCN1A expression after AntagoNAT treatment of different Dravet mutations. (a) SCN1A mRNA levels in 5 Dravet patient fibroblast lines treated with 20 nM of CUR-1916; normalized to inactive oligonucleotide control, real time PCR data, *t*-test with Bonferroni correction, $n = 18$/group. (b) Copy numbers of WT and mutant (X) SCN1A mRNAs in fibroblast lines D-00 and D-02. Mutant mRNA was undetectable in both cell lines (allele-specific real time PCR with synthetic copy number standards, $n = 3$ wells/group). Mean ± S.E.M., ** − $p < 0.01$, *** − $p < 0.001$.

seizure thresholds were significantly lower than in WT mice (40.6 ± 0.3 °C and 43.2 ± 0.1 °C respectively). To test if increasing Scn1a expression after birth can affect the heat-induced seizure threshold, we intrathecally injected 7 week-old Scn1a$^{E1099X/+}$ mice weekly with 1 μg of CUR-1901, or an equal volume of saline, for 4 weeks. The heat induction test was conducted 3 days after the last injection. Seizure threshold temperature in CUR-1901-treated mice was significantly increased compared to vehicle controls (41.42 ± 0.26 and 40.15 ± 0.27, $n = 4$ and $n = 6$ respectively, *t*-test $p = 0.01$, Fig. 9). Threshold temperatures in WT mice did not change significantly after AntagoNAT treatment compared to vehicle-treated mice (43.6 ± 0.16 °C and 43.8 ± 0.1 °C respectively, Fig. 9b).

Overall, these results indicate that increasing Scn1a expression in adult Dravet mice can reduce sensitivity to heat-induced seizures.

3.8. Upregulation of Scn1a in Dravet Mice Normalizes Excitability of Parvalbumin Interneurons

In previous mouse models of Dravet, seizure phenotype correlated with reduced excitability in hippocampal interneurons (Mistry et al., 2014; Tai et al., 2014; Cheah et al., 2012). To determine if upregulated Scn1a expression observed in our experiments affects neuronal excitability, we investigated firing characteristics of parvalbumin (PV)-
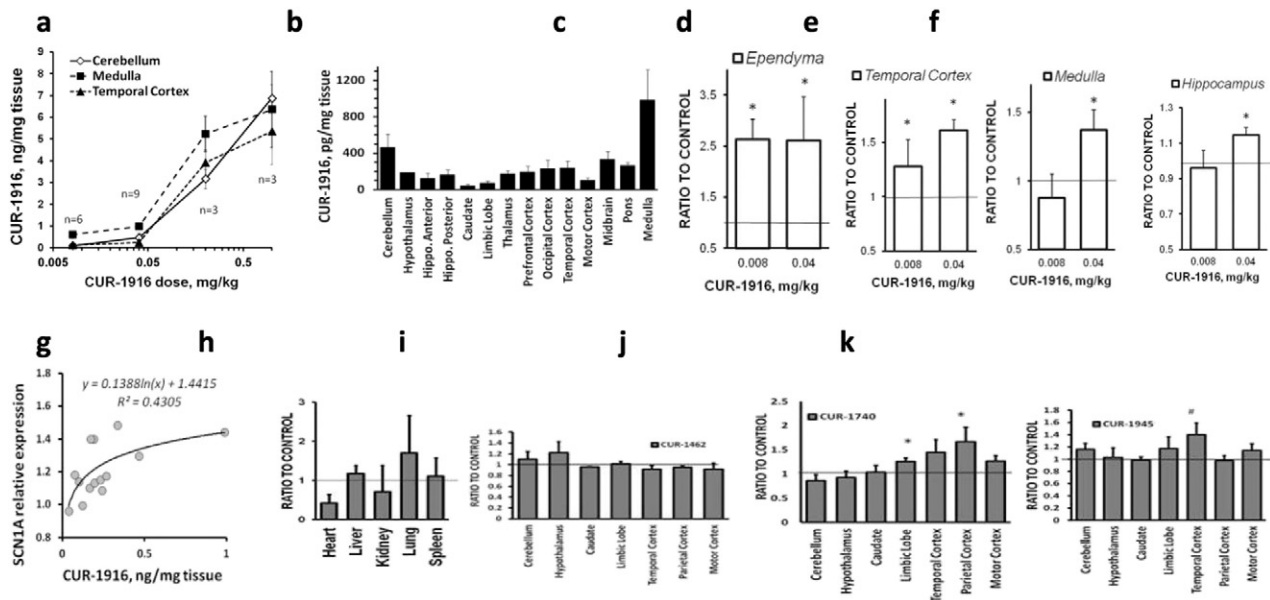
Fig. 12. AntagoNAT distribution and Scn1a upregulation in vivo in African green monkeys. Animals were injected IT with different doses of CUR-1916. (a) Tissue concentration of CUR-1916 in monkey brain 7 days after injection (hybridization assay data). (b) CUR-1916 concentrations in different monkey brain regions after treatment with 0.04 mg/kg of CUR-1916 (hybridization assay data, $n = 9$). (c–f) Upregulation of Scn1a mRNA in brain regions ($n = 6$ for 0.008 mg/kg, $n = 9$ for 0 and 0.04 mg/kg of CUR-1916; real time PCR data, ANOVA $p < 0.05$). (g) Correlation of CUR-1916 concentration in tissues with Scn1a upregulation levels (regression $p = 0.02$). (h) Scn1a expression levels in peripheral organs in monkeys treated with 0.04 mg/kg of CUR-1916 (ANOVA $p > 0.1$, $n = 6$/group). (i–k) Scn1a mRNA expression levels in CNS regions of monkeys treated IT with 0.04 mg/kg of: (i) an inactive oligonucleotide CUR-1462 (normalized to saline control, ANOVA $p = 0.21$, $n = 7$ for CUR-1462, 9 for saline); (j) human-specific AntagoNAT CUR-1740 (normalized to CUR-1462, ANOVA $p = 0.05$, $n = 4$); (k) human-specific AntagoNAT CUR-1945 (normalized to CUR-1462, ANOVA $p = 0.1$, $n = 4$). Mean ± S.E.M., * − $p < 0.05$, # − $p < 0.1$. Mean ± S.E.M., * − $p < 0.05$.

positive GABAergic interneurons in acute hippocampal slices of AntagoNAT-treated and control Scn1a$^{E1099X/+}$ mice. PV-positive interneurons were recognized by their large soma (>30 μm), fast spiking and localization at the border of the granule cell layer in the dentate gyrus (DG), and later confirmed by IHC staining for PV. The activity of PV-positive interneurons was recorded under current clamp in 5–6 week old mice, 4 days after a single IT injection of 5 μg of CUR-1901. Compared to WT, the Scn1a$^{E1099X/+}$ control mice had higher current threshold to first action potential (AP) and impaired AP firing frequencies (Fig. 10a, b). These deficits were significantly improved after CUR-1901 treatment, with both AP firing threshold and firing frequency restored to values approaching WT (Fig. 10a, b). Furthermore, AP characteristics which were significantly altered in Dravet mice, including AP half-width, rise slope, decay slope and amplitude, returned to WT levels after treatment with AntagoNAT, with decay slope and amplitude slightly exceeding WT values (Fig. 10c-f). Decreased amplitude of afterhyperpolarization (AHP) observed in Scn1a$^{E1099X/+}$ mice compared to WT, was not affected by the AntagoNAT treatment (Fig. 10g). This could be explained by the short duration of the experiment (78 h), not sufficient to alter the adaptive changes in BK channels, which are the major contributors to AHP. Our RNAseq data also showed that short-term Scn1a upregulation was not accompanied by changes in expression of BK channel subunits (Supplementary File 1). Input resistance and resting potential were not significantly altered in any group (Fig. 10h, i; Table 4).

Taken together, these data indicate that increasing Scn1a expression in adult mice is associated with improved electrophysiological characteristics of PV-positive hippocampal interneurons, which are essential for the pathophysiology of Dravet.

3.9. AntagoNAT Treatment Upregulates SCN1A in Cells With Diverse Dravet Mutations

Dravet syndrome is caused by a wide variety of de novo mutations, which are rarely inherited. To determine if same AntagoNAT can upregulate SCN1A in cells with different mutation types, we treated primary fibroblasts from 5 patients with 20 nM of a human-specific AntagoNAT CUR-1916 or an inactive control oligonucleotide of similar chemistry. Mutation types were nonsense, missense, frame shift and short duplication (Table 5). In all fibroblast lines SCN1A mRNA levels were increased after AntagoNAT treatment by at least 10 fold, and up to 40 fold, compared to control (real time PCR data, ANOVA $p > 0.001$, $n = 18$/group, Fig. 11a). Notably, the D-02 line, showing the highest upregulation of SCN1A upon AntagoNAT treatment, had a much lower basal SCN1A level compared to D-00 line (Fig. 11b). Using allele-specific gene-expression assays with synthetic calibration standards we determined that mutant SCN1A mRNA was not detectable in either D-00 or D-02 line (Fig. 11b).

Overall, these results indicate that AntagoNAT-mediated inhibition of SCN1ANAT results in the upregulation of SCN1A regardless of the SCN1A mutation type, thus increasing potential applicability of the AntagoNAT method in the treatment of Dravet syndrome and other diseases caused by de-novo mutations.

3.10. Intrathecal Injection of Human AntagoNATs Upregulates Scn1a in Non-human Primate Brain

As mouse and human SCN1ANATs do not share significant sequence similarity, we had to use mouse-specific AntagoNATs in our experiments in Dravet mice. To determine if their human-specific counterparts would have the same effect on Scn1a expression in vivo, we employed African green monkey model, whose Scn1aNAT is highly homologous to human (Table 1). Furthermore, human-specific AntagoNATs induced gene-specific Scn1a mRNA and protein upregulation in an African green monkey cell line Vero76 (Figs. 4b, 5h). Besides species-specificity, other issue that could be addressed in the African

green monkey model was absorption, distribution and cellular availability and safety of AntagoNATs after IT administration, because CNS anatomy and physiology of non-human primates closely resembles human.

We injected African green monkeys once IT with saline vehicle, inactive control oligonucleotide or active primate-specific AntagoNATs at 1, 0.2, 0.04 or 0.008 mg/kg doses. The animals were sacrificed 1 week after injection. The resulting tissue concentrations of AntagoNAT CUR-1916 varied depending on injected amount, exposure to CSF circulation and proximity to injection site (Fig. 12a, b). Seven days after injection of 0.008 and 0.04 mg/kg doses, concentrations of the full length CUR-1916 were 45% and 16%, respectively, of the maximum possible assuming even distribution of AntagoNAT over CNS volume. AntagoNAT concentrations in the CSF seven days after injection were 5.27 ± 1.99 ng/ml at the 0.008 mg/kg dose and 16.79 ± 4.12 ng/ml at 0.04 mg/kg ($n = 6$). In plasma after 7 days CUR-1916 was undetectable at doses below 1 mg/kg, where it equaled 0.15 ± 0.05 ng/ml ($n = 3$). CUR-1916 was also undetectable in peripheral organs including heart, lung and spleen, at and below 0.2 mg/kg ($n = 9$). In kidney the concentration was below quantitation limit at 0.008 mg/kg ($n = 6$) and 0.04 mg/kg ($n = 9$); at 0.2 and 1 mg/kg it was 0.27 ± 0.04 and 0.34 ± 0.05 ng/mg tissue respectively ($n = 3$). Confocal microscopy demonstrated that CUR-1916 was present inside hippocampal parvalbumin-positive neurons, which are central to Dravet pathogenesis (video in Supplementary File 4).

Brain Scn1a mRNA levels measured seven days after IT injection of CUR-1916 were upregulated in dose-dependent fashion compared to vehicle and inactive oligonucleotide controls, with the largest increase observed in ependyma (250%, ANOVA $p < 0.05$; Fig. 12c-f). The average levels of Scn1a upregulation in brain regions followed the observed local AntagoNAT concentration with EC50 of approximately 0.22 ng CUR-1916/mg tissue ($r^2 = 0.43$, $p = 0.01$; Fig. 12g). In peripheral tissues no significant effect of AntagoNAT treatment on Scn1a mRNA levels was observed (ANOVA $p > 0.1$; Fig. 12h). To confirm that AntagoNAT effect was target-specific, we treated monkeys IT with 0.04 mg/kg of CUR-1740 or CUR-1945 (active AntagoNATs with different chemistry and sequences) or CUR-1462 (an inactive oligonucleotide). While Scn1a expression after treatment with CUR-1462 did not differ from vehicle control (ANOVA $p = 0.21$, $n = 3$/group), the active AntagoNATs induced statistically significant upregulation, or upregulation trends in Scn1a expression (+15 to +60%; $n = 3$/group, Fig. 12i–k).

Histopathological examination of brains of animals one week after treatment with different doses of CUR-1916 revealed no AntagoNAT-associated histopathology.

Overall, the experiments in African green monkeys indicate that human AntagoNATs injected IT in saline vehicle can induce specific Scn1a upregulation in vivo in a CNS closely resembling human. The experiments also demonstrate that AntagoNATs injected IT are largely safe and contained within CNS, reducing the possibility of peripheral side effects.

4. Discussion

At present time the majority of genetic disorders involving haploinsufficiency in a single gene, such as Dravet syndrome, have no adequate treatment. Only partially effective symptomatic therapy targeted at seizure reduction is now available for Dravet patients. Furthermore, although initially Dravet syndrome was considered an epileptic encephalopathy (Wolff et al., 2006), recent studies in Dravet patients have shown that some aspects of the syndrome may arise independently of seizures and thus cannot be addressed by anticonvulsants (Nabbout et al., 2013). In rat models, siRNA-mediated Scn1a knockdown in adult animals selective for basal forebrain induced cognitive impairment without seizures (Bender et al., 2013). Notably, upregulation of the remaining normal copy of the damaged gene has the potential to improve all disease manifestations and represents an appealing therapeutic strategy.

In our studies we have demonstrated a new regulatory mechanism of SCN1A expression, mediated by a gene-specific NAT, and showed that blocking this NAT can be used to achieve specific SCN1A upregulation in cells, including cells heterozygous for Dravet mutations. These results indicate that NAT-mediated regulation is not engaged, or at least not tapped out, in haploinsufficient cells, possibly due to lack of the feedback from SCN1A protein levels. NAT-mediated expression control is present in many disease-relevant loci and can potentially be used in the treatment of multiple haploinsufficiency-linked genetic disorders and other diseases where upregulation of disease-causing gene can be beneficial.

In our *in vitro* and *in vivo* experiments we were able to upregulate SCN1A expression by using AntagoNATs (oligonucleotide-like compounds) that block the activity of SCN1ANAT. While AntagoNAT treatment upregulated SCN1A, it did not affect >90% of all expressed genes, including other highly homologous sodium channel subunits and genes immediately adjacent to SCN1A on the chromosome (Fig. 5; Supplementary File 1).

Furthermore, we have demonstrated that SCN1A upregulation can be effective in a mouse model of Dravet if applied at some time point after birth, when genetic disorders are usually diagnosed. Our experiments in a mouse model harboring a known Dravet mutation demonstrate that Scn1a upregulation during PW 7–11 leads to improvements in several aspects of disease phenotype, including frequency and severity of seizures. We observed that a 25% increase in brain Scn1a levels was sufficient to elicit a 70% reduction in seizure frequency and a decrease in seizure severity (Fig. 8). Additionally, upregulation of brain Scn1a levels was associated with decreased sensitivity to heat-induced seizures, which represent a hallmark of Dravet syndrome. AntagoNAT treatment also normalized increased firing threshold and reduced firing frequency of inhibitory interneurons observed in Dravet models (Fig. 9, Oakley et al., 2011; Yamakawa, 2011; Tai et al., 2014; Ogiwara et al., 2013). Importantly, in rat models with RNAi-induced Scn1a knockdown, disruption in neuronal firing was correlated with performance in working memory task (Bender et al., 2016). This underscores the importance of normalizing the neuronal firing for the treatment of cognitive deficits associated with Dravet syndrome. Overall, significant improvements of seizure phenotype and neuronal electrophysiology observed in our experiments provide an integral indicator that Scn1a upregulation achieved using AntagoNATs can adequately address the excitation/inhibition imbalance occurring in Dravet brain.

Besides seizures, another known aspect of Dravet syndrome is increased mortality (Dravet, 2011). Similar to human disease, the death rate in the Scn1a$^{E1099X/+}$ mice peaks in early development (with approximately 70% of mice dying before PW7) and then stabilizes at relatively low levels. Additionally, Dravet mice are generally smaller and have elevated sensitivity to surgical interventions compared to WT. For these reasons, in our experiments EEG electrode implantation and IT injection of AntagoNATs were conducted at PW7–11, past the critical period. As a result, the small numbers of deaths observed in our studies did not allow for a conclusive statistical analysis at this time. Consequently, the reported results are only relevant to the more mildly affected surviving mice or potentially Dravet patients older than 3 years. Further experiments, in which AntagoNAT treatment will be started prior to the PW3–5 critical window are needed to verify whether AntagoNAT-mediated upregulation of SCN1A could reduce the early mortality rate. Due to technical difficulties, these experiments would likely require development of an alternative administration route.

Further experiments are underway to test if the increase in Scn1a levels in a Dravet mouse model would affect other Dravet manifestations, such as delayed psychomotor development and autistic-like behavior. Taken together, our results demonstrate that at least some of the major aspects of Dravet are likely to be caused by persistent SCN1A deficit after birth and can be improved by AntagoNAT-mediated upregulation of SCN1A.

Additionally, we showed that treatment with the same AntagoNAT induced SCN1A upregulation in human cells with different mutation types (Fig. 11), thus opening the possibility of using one AntagoNAT for the treatment of many Dravet patients, as opposed to designing a separate molecule for each mutation. This aspect is particularly relevant in Dravet syndrome, which is usually caused by de novo mutations. Furthermore, the cost of the initial screening of AntagoNATs is substantially lower compared to small molecules, which makes AntagoNATs highly amenable for the treatment of genetic disorders will small patient populations.

Given the significant differences in the anatomy and physiology of human and rodent CNS and the diversity in the sequences of human and mouse SCN1ANATs, we also tested the effects of human-specific AntagoNATs in a non-human primate model (Fig. 12). Primates have high SCN1ANAT sequence conservation and their CNS anatomy and physiology closely resembles human. A single IT injection of the human-specific AntagoNAT CUR-1916 in saline vehicle induced dose-dependent increase of Scn1a expression in the brain of African green monkeys (Fig. 12c–f). At the same time, we observed intracellular localization of AntagoNATs inside hippocampal parvalbumin positive neurons, which are essential to Dravet pathophysiology and represent an important cellular target for therapeutic upregulation of SCN1A (video in Supplementary File 4). The observed sequestration of AntagoNATs in the CNS after IT administration will likely reduce the possibility of side effects in peripheral organs. Additionally, the in vivo doses of AntagoNATs which induced significant upregulation of Scn1a in our experiments were approximately 10-fold lower than active doses reported for oligonucleotides with other mechanisms of action (Miller et al., 2013; Flanigan et al., 2014). Using lower doses would further reduce the chances of adverse events. Taken together these results indicate that IT administration of AntagoNATs may be a viable route for upregulating SCN1A expression in the clinic.

5. Conclusions

Overall, our results show that gene upregulation through blocking the inhibitory activity of NATs by AntagoNAT treatment may improve several aspects of Dravet syndrome. Furthermore we demonstrate that IT injection in a saline vehicle is safe and represents a viable administration route for AntagoNATs in the clinic. As large proportion of protein loci are regulated by NATs, NAT-targeted therapies can be applied in many currently untreatable human genetic disorders associated with haploinsufficiency and other diseases which can benefit from gene upregulation.

Supplementary data to this article can be found online at http://dx.doi.org/10.1016/j.ebiom.2016.05.011.

References

Bechi, G., Scalmani, P., Schiavon, E., Rusconi, R., Franceschetti, S., Mantegazza, M., 2011. Pure halopinsufficiency for Dravet syndrome Nav1.1 (SCN1A) sodium channel truncating mutations. Epilepsia (1528-1167 PMID: 22150645).

Bender, A.C., Natola, H., Ndong, C., Holmes, G.L., Scott, R.C., Lenck-Santini, P.P., 2013. Focal Scn1a knockdown induces cognitive impairment without seizures. Neurobiol. Dis. 54, 297–307 (Jun PMID: 23318929).

Bender, A.C., Luikart, B.W., Lenck-Santini, P.P., 2016. Cognitive deficits associated with Nav1.1 alterations: involvement of neuronal firing dynamics and oscillations. PLoS One 11 (3), e0151538. http://dx.doi.org/10.1371/journal.pone.0151538 (Mar 15, eCollection 2016. PMID: 26978272).

BrainSpan Atlas, d. http://www.brainspan.org (accessed 05/02/2016).

Cahoy, J.D., Emery, B., Kaushal, A., Foo, L.C., Zamanian, J.L., Christopherson, K.S., Xing, Y., Lubischer, J.L., Krieg, P.A., Krupenko, S.A., Thompson, W.J., Barres, B.A., 2008. A transcriptome database for astrocytes, neurons, and oligodendrocytes: a new resource for understanding brain development and function. J. Neurosci. 28 (1), 264–278. http://dx.doi.org/10.1523/JNEUROSCI.4178-07.2008 (Jan 2).

Cheah, C.S., Yu, F.H., Westenbroek, R.E., Kalume, F.K., Oakley, J.C., Potter, G.B., Rubenstein, J.L., Catterall, W.A., 2012. Specific deletion of NaV1.1 sodium channels in inhibitory interneurons causes seizures and premature death in a mouse model of Dravet syndrome. Proc. Natl. Acad. Sci. U. S. A. 109 (36), 14646–14651 (Sep 4 PMID: 22908258).

Cheah, C.S., Westenbroek, R.E., Roden, W.H., Kalume, F., Oakley, J.C., Jansen, L.A., Catterall, W.A., 2013. Correlations in timing of sodium channel expression, epilepsy, and sudden death in Dravet syndrome. Channels (Austin) 7 (6), 468–472. http://dx.doi.org/10.4161/chan.26023 (Nov-Dec Epub 2013 Aug 21. PMID: 23965409).

Chung, D.W., Rudnicki, D.D., Yu, L, Margolis, R.L., 2011. A natural antisense transcript at the Huntington's disease repeat locus regulates HTT expression. Hum. Mol. Genet. 20 (17), 3467–3477. http://dx.doi.org/10.1093/hmg/ddr263 (Sep 1 Epub 2011 Jun 13. PMID: 21672921).

Davidovich, C., Zheng, L., Goodrich, K.J., Cech, T.R., 2013. Promiscuous RNA binding by polycomb repressive complex 2. Nat. Struct. Mol. Biol. 20 (11), 1250–1257 (Nov PMID: 24077223).

Derrien, T., Johnson, R., Bussotti, G., Tanzer, A., Djebali, S., Tilgner, H., Guernec, G., Martin, D., Merkel, A., Knowles, D.G., Lagarde, J., Veeravalli, L., Ruan, X., Ruan, Y., Lassmann, T., Carninci, P., Brown, J.B., Lipovich, L., Gonzalez, J.M., Thomas, M., Davis, C.A., Shiekhattar, R., Gingeras, T.R., Hubbard, T.J., Notredame, C., Harrow, J., Guigó, R., 2012. The GENCODE v7 catalog of human long noncoding RNAs: analysis of their gene structure, evolution, and expression. Genome Res. 22 (9), 1775–1789 (PMID: 22955988).

Dravet, C., 2011. The core Dravet syndrome phenotype. Epilepsia 52 (Suppl. 2), 3–9 (Apr PMID: 21463272).

Flanigan, K.M., Voit, T., Rosales, X.Q., Servais, L., Kraus, J.E., Wardell, C., Morgan, A., Dorricott, S., Nakielny, J., Quarcoo, N., Liefaard, L., Drury, T., Campion, G., Wright, P., 2014. Pharmacokinetics and safety of single doses of drisapersen in non-ambulant subjects with Duchenne muscular dystrophy: results of a double-blind randomized clinical trial. Neuromuscul. Disord. 24 (1), 16–24. http://dx.doi.org/10.1016/j.nmd.2013.09.004 (Jan Epub 2013 Sep 11.PMID: 24321394).

GNF Expression Atlas 2, d. http://genome.ucsc.edu/cgi-bin/hgGene?hgg_gene=uc021vsb.1&hgg_prot=P354982&hgg_chrom=chr2&hgg_start=166845669&hgg_end=166930180&hgg_type=knownGene&db=hg19&hgsid=337727395 (accessed January 4 2014).

Goeggel Simonetti, B., Rieubland, C., Courage, C., Strozzi, S., Tschumi, S., Gallati, S., Lemke, J.R., 2012. Duplication of the sodium channel gene cluster on 2q24 in children with early onset epilepsy. Epilepsia 53 (12), 2128–2134. http://dx.doi.org/10.1111/j.1528-1167.2012.03676.x (Dec Epub 2012 Sep 27. PMID: 23016767).

Gruber, A.R., Lorenz, R., Bernhart, S.H., Neuböck, R., Hofacker, I.L., 2008. The Vienna RNA websuite. Nucleic Acids Res. 36 (Web Server issue), W70–W74. http://dx.doi.org/10.1093/nar/gkn188 (Jul 1 Epub 2008 Apr 19).

Halley, P., Kadakkuzha, B.M., Faghihi, M.A., Magistri, M., Zeier, Z., Khorkova, O., Coito, C., Hsiao, J., Lawrence, M., Wahlestedt, C., 2014. Regulation of the apolipoprotein gene cluster by a long noncoding RNA. Cell Rep. 6 (1), 222–230 (Jan 16 PMID: 24388749).

Hylden, J.L., Wilcox, G.L., 1980. Intrathecal morphine in mice: a new technique. Eur. J. Pharmacol. 67 (2–3), 313–316 (Oct 17 PMID: 6893963).

Kalume, F., Westenbroek, R.E., Cheah, C.S., Yu, F.H., Oakley, J.C., Scheuer, T., Catterall, W.A., 2013. Sudden unexpected death in a mouse model of Dravet syndrome. J. Clin. Invest. 123 (4), 1798–1808 (Apr 1 PMID: 23524966).

Katayama, S., Tomaru, Y., Kasukawa, T., Waki, K., Nakanishi, M., Nakamura, M., Nishida, H., Yap, C.C., Suzuki, M., Kawai, J., Suzuki, H., Carninci, P., Hayashizaki, Y., Wells, C., Frith, M., Ravasi, T., Pang, K.C., Hallinan, J., Mattick, J., Hume, D.A., Lipovich, L., Batalov, S., Engström, P.G., Mizuno, Y., Faghihi, M.A., Sandelin, A., Chalk, A.M., Mottagui-Tabar, S., Liang, Z., Lenhard, B., Wahlestedt, C., Genome Exploration Research Group, R.I.K.E.N., Genome Science Group (Genome Network Project Core Group), 2005. FANTOM Consortium. Antisense transcription in the mammalian transcriptome. Science 309 (5740), 1564–1566 (Sep 2 PMID: 16141073).

Khalil, A.M., Guttman, M., Huarte, M., Garber, M., Raj, A., Rivea Morales, D., Thomas, K., Presser, A., Bernstein, B.E., van Oudenaarden, A., Regev, A., Lander, E.S., Rinn, J.L., 2009. Many human large intergenic noncoding RNAs associate with chromatin-modifying complexes and affect gene expression. Proc. Natl. Acad. Sci. U. S. A. 106 (28), 11667–11672 (Jul 14 PMID: 19571010).

Kim, S.H., Nordli Jr., D.R., Berg, A.T., Koh, S., Laux, L., 2014. Ictal ontogeny in Dravet syndrome. Clin. Neurophysiol. (Jun 30 pii: S1388-2457(14)00336-8. PMID: 25046982).

Kotake, Y., Nakagawa, T., Kitagawa, K., Suzuki, S., Liu, N., Kitagawa, M., Xiong, Y., 2011. Long non-coding RNA ANRIL is required for the PRC2 recruitment to and silencing of p15(INK4B) tumor suppressor gene. Oncogene 30 (16), 1956–1962 (Apr 21 PMID: 21151178).

Landis, S.C., Amara, S.G., Asadullah, K., et al., 2012. A call for transparent reporting to optimize the predictive value of preclinical research. Nature 490 (7419), 187–191. http://dx.doi.org/10.1038/nature11556.

Liautard, C., Scalmani, P., Carriero, G., de Curtis, M., Franceschetti, S., Mantegazza, M., 2013. Hippocampal hyperexcitability and specific epileptiform activity in a mouse model of Dravet syndrome. Epilepsia 54 (7), 1251–1261 (Jul PMID: 23663038).

Liu, P., Jenkins, N.A., Copeland, N.G., 2003. A highly efficient recombineering-based method for generating conditional knockout mutations. Genome Res. 13 (3), 476–484 (Mar PMID: 12618378).

Magistri, M., Faghihi, M.A., St Laurent 3rd, G., Wahlestedt, C., 2012. Regulation of chromatin structure by long noncoding RNAs: focus on natural antisense transcripts. Trends Genet. 28 (8), 389–396 (Aug PMID: 22541732).

Martin, M.S., Dutt, K., Papale, L.A., Dubé, C.M., Dutton, S.B., de Haan, G., Shankar, A., Tufik, S., Meisler, M.H., Baram, T.Z., Goldin, A.L., Escayg, A., 2010. Altered function of the SCN1A voltage-gated sodium channel leads to gamma-aminobutyric acid-ergic (GABAergic) interneuron abnormalities. J. Biol. Chem. 285 (13), 9823–9834 (PMID: 20100831).

Matsui, M., Chu, Y., Zhang, H., Gagnon, K.T., Shaikh, S., Kuchimanchi, S., Manoharan, M., Corey, D.R., Janowski, B.A., 2013. Promoter RNA links transcriptional regulation of inflammatory pathway genes. Nucleic Acids Res. 41 (22), 10086–10109. http://dx.doi.org/10.1093/nar/gkt777 (Dec Epub 2013 Sep 2.PMID: 23999091).

Meng, L., Ward, A.J., Chun, S., Bennett, C.F., Beaudet, A.L., Rigo, F., 2015. Towards a therapy for Angelman syndrome by targeting a long non-coding RNA. Nature 518 (7539), 409–412. http://dx.doi.org/10.1038/nature13975 (Feb 19 Epub 2014 Dec 1. PMID: 25470045).

Miller, T.M., Pestronk, A., David, W., Rothstein, J., Simpson, E., Appel, S.H., Andres, P.L., Mahoney, K., Allred, P., Alexander, K., Ostrow, L.W., Schoenfeld, D., Macklin, E.A., Norris, D.A., Manousakis, G., Crisp, M., Smith, R., Bennett, C.F., Bishop, K.M., Cudkowicz, M.E., 2013. An antisense oligonucleotide against SOD1 delivered intrathecally for patients with SOD1 familial amyotrophic lateral sclerosis: a phase 1, randomised, first-in-man study. Lancet Neurol. 12 (5), 435–442 (May PMID: 23541756).

Mistry, A.M., Thompson, C.H., Miller, A.R., Vanoye, C.G., George Jr., A.L., Kearney, J.A., 2014. Strain- and age-dependent hippocampal neuron sodium currents correlate with epilepsy severity in Dravet syndrome mice. Neurobiol. Dis. 65, 1–11 (May PMID: 24434335).

Modarresi, F., Faghihi, M.A., Lopez-Toledano, M.A., Fatemi, R.P., Magistri, M., Brothers, S.P., van der Brug, M.P., Wahlestedt, C., 2012. Inhibition of natural antisense transcripts in vivo results in gene-specific transcriptional upregulation. Nat. Biotechnol. 30 (5), 453–459 (Apr 25 PMID: 22446693).

Mortazavi, A., Williams, B.A., McCue, K., Schaeffer, L., Wold, B., 2008. Mapping and quantifying mammalian transcriptomes by RNA-Seq. Nat. Methods 5 (7), 621–628. http://dx.doi.org/10.1038/nmeth.1226 (Jul Epub 2008 May 30. PMID: 18516045).

Nabbout, R., Chemaly, N., Chipaux, M., Barcia, G., Bouis, C., Dubouch, C., Leunen, D., Jambaqué, I., Dulac, O., Dellatolas, G., Chiron, C., 2013. Encephalopathy in children with Dravet syndrome is not a pure consequence of epilepsy. Orphanet J. Rare Dis. 8, 176 (Nov 13 PMID: 24225340).

Nakagawa, S., Kageyama, Y., 2014. Nuclear lncRNAs as epigenetic regulators-beyond skepticism. Biochim. Biophys. Acta 1839 (3), 215–222 (Mar PMID: 24200874).

Oakley, J.C., Kalume, F., Catterall, W.A., 2011. Insights into pathophysiology and therapy from a mouse model of Dravet syndrome. Epilepsia 52 (Suppl. 2), 59–61 (Apr PMID: 21463282).

Ogiwara, I., Miyamoto, H., Morita, N., Atapour, N., Mazaki, E., Inoue, I., Takeuchi, T., Itohara, S., Yanagawa, Y., Obata, K., Furuichi, T., Hensch, T.K., Yamakawa, K., 2007. Nav1.1 localizes to axons of parvalbumin-positive inhibitory interneurons: a circuit basis for epileptic seizures in mice carrying an Scn1a gene mutation. J. Neurosci. 27 (22), 5903–5914 (PMID: 17537961).

Ogiwara, I., Iwasato, T., Miyamoto, H., Iwata, R., Yamagata, T., Mazaki, E., Yanagawa, Y., Tamamaki, N., Hensch, T.K., Itohara, S., Yamakawa, K., 2013. Nav1.1 haploinsufficiency in excitatory neurons ameliorates seizure-associated sudden death in a mouse model of Dravet syndrome. Hum. Mol. Genet. 22 (23), 4784–4804. http://dx.doi.org/10.1093/hmg/ddt331 (Dec 1 Epub 2013 Aug 6. PMID: 23922229).

Ohmori, I., Kahlig, K.M., Rhodes, T.H., Wang, D.W., AL Jr., G., 2006. Nonfunctional SCN1A is common in severe myoclonic epilepsy of infancy. Epilepsia 47 (10), 1636–1642 (Oct PMID: 17054685).

Peschansky, V.J., Wahlestedt, C., 2014. Non-coding RNAs as direct and indirect modulators of epigenetic regulation. Epigenetics 9 (1), 3–12. http://dx.doi.org/10.4161/epi.27473 (Jan, PMID: 24739571).

Preacher, K.J., Briggs, N.E., 2001. Calculation for Fisher's Exact Test: an interactive calculation tool for Fisher's exact probability test for 2 × 2 tables [computer software]. Available from http://quantpsy.org.

Sugawara, T., Tsurubuchi, Y., Fujiwara, T., Mazaki-Miyazaki, E., Nagata, K., Montal, M., Inoue, Y., Yamakawa, K., 2003. Nav1.1 channels with mutations of severe myoclonic epilepsy in infancy display attenuated currents. Epilepsy Res. 54, 201–207.

Tai, C., Abe, Y., Westenbroek, R.E., Scheuer, T., Catterall, W.A., 2014. Impaired excitability of somatostatin- and parvalbumin-expressing cortical interneurons in a mouse model of Dravet syndrome. Proc. Natl. Acad. Sci. U. S. A. 111 (30), E3139–E3148. http://dx.doi.org/10.1073/pnas.1411131111 (Jul 29 Epub 2014 Jul 14. PMID: 25024183).

Taylor, J.R., Elsworth, J.D., Roth, R.H., Sladek Jr., J.R., Redmond Jr., D.E., 1997. Severe long-term 1-methyl-4-phenyl-1,2,3,6-tetrahydropyridine-induced parkinsonism in the vervet monkey (Cercopithecus aethiops sabaeus). Neuroscience 81 (3), 745–755 (Dec PMID: 9316026).

The Human Protein Atlas, d. http://www.proteinatlas.org/ENSG00000144285 (accessed January 4 2014).

Thiele, C.J., 1998. In: Masters, J. (Ed.), NeuroblastomaHuman Cell Culture vol. 1. Kluwer Academic Publishers, Lancaster, UK, pp. 21–53 (http://home.ccr.cancer.gov/oncology/oncogenomics/Papers/Neuroblastoma%20Cell%20Lines%20–%20Molecular%20Features.pdf).

Tsai, M.S., Lee, M.L., Chang, C.Y., Fan, H.H., Yu, I.S., Chen, Y.T., You, J.Y., Chen, C.Y., Chang, F.C., Hsiao, J.H., Khorkova, O., Liou, H.H., Yanagawa, Y., Lee, L.J., Lin, S.W., 2015. Functional and structural deficits of the dentate gyrus network coincide with emerging spontaneous seizures in an Scn1a mutant Dravet Syndrome model during development. Neurobiol. Dis. 77, 35–48. http://dx.doi.org/10.1016/j.nbd.2015.02.010 (May Epub 2015 Feb 26. PMID: 25725421).

Vanoye, C.G., Lossin, C., Rhodes, T.H., George Jr., A.L., 2006. Single-channel properties of human NaV1.1 and mechanism of channel dysfunction in SCN1A-associated epilepsy. J. Gen. Physiol. 127 (1), 1–14 (Jan PMID: 16380441).

Wahlestedt, C., 2013. Targeting long non-coding RNA to therapeutically upregulate gene expression. Nat. Rev. Drug Discov. 12 (6), 433–446 (Jun PMID: 23722346).

Wolff, M., Cassé-Perrot, C., Dravet, C., 2006. Severe myoclonic epilepsy of infants (Dravet syndrome): natural history and neuropsychological findings. Epilepsia 47 (Suppl. 2), 45–48 (PMID: 17105460).

Yamakawa, K., 2011. Molecular and cellular basis: insights from experimental models of Dravet syndrome. Epilepsia 52 (Suppl. 2), 70–71 (Apr PMID: 21463284).

Yamanaka, Y., Faghihi, M.A., Magistri, M., Alvarez-Garcia, O., Lotz, M., Wahlestedt, C., 2015. Antisense RNA controls LRP1 sense transcript expression through interaction with a chromatin-associated protein, HMGB2. Cell Rep. 11 (6), 967–976. http://dx.doi.org/10.1016/j.celrep.2015.04.011 (May 12 Epub 2015 Apr 30.PMID: 25937287).

Yoshitomi, S., Takahashi, Y., Ishizuka, M., Yamaguchi, T., Watanabe, A., Nasu, H., Ueda, Y., Ohtani, H., Ikeda, H., Imai, K., Shigematsu, H., Inoue, Y., Tanahashi, Y., Aiba, K., Ohta, H., Shimada, S., Yamamoto, T., 2015. Three patients manifesting early infantile epileptic spasms associated with 2q24.3 microduplications. Brain Dev. (Apr 2 pii: S0387-7604(15)00063-7. PMID: 25843248).

Yu, F.H., Mantegazza, M., Westenbroek, R.E., Robbins, C.A., Kalume, F., Burton, K.A., Spain, W.J., McKnight, G.S., Scheuer, T., Catterall, W.A., 2006. Reduced sodium current in GABAergic interneurons in a mouse model of severe myoclonic epilepsy in infancy. Nat. Neurosci. 9 (9), 1142–1149 (PMID: 16921370).

Yu, A.D., Wang, Z., Morris, K.V., 2015. Long noncoding RNAs: a potent source of regulation in immunity and disease. Immunol. Cell Biol. 93 (3), 277–283. http://dx.doi.org/10.1038/icb.2015.2 (Mar, PMID: 25776990).

Zhao, J., Ohsumi, T.K., Kung, J.T., Ogawa, Y., Grau, D.J., Sarma, K., Song, J.J., Kingston, R.E., Borowsky, M., Lee, J.T., 2010. Genome-wide identification of polycomb-associated RNAs by RIP-seq. Mol. Cell 40 (6), 939–953 (Dec 22 PMID: 21172659).